

Accepted Manuscript

Geological Society, London, Special Publications

Explosive sequence of La Soufrière St Vincent April 2021: insights into drivers and consequences via eruptive products

P. D. Cole, J. Barclay, R. E. A. Robertson, S. Mitchell, B. V. Davies, R. Constantinescu, R. S. J. Sparks, W. Aspinall & A. Stinton

DOI: <https://doi.org/10.1144/SP539-2022-292>

To access the most recent version of this article, please click the DOI URL in the line above. When citing this article please include the above DOI.

Received 23 September 2022

Revised 20 December 2022

Accepted 3 January 2023

© 2023 The Author(s). This is an Open Access article distributed under the terms of the Creative Commons Attribution 4.0 License (<http://creativecommons.org/licenses/by/4.0/>). Published by The Geological Society of London. Publishing disclaimer: www.geolsoc.org.uk/pub_ethics

Supplementary material at <https://doi.org/10.6084/m9.figshare.c.6474317>

Manuscript version: Accepted Manuscript

This is a PDF of an unedited manuscript that has been accepted for publication. The manuscript will undergo copyediting, typesetting and correction before it is published in its final form. Please note that during the production process errors may be discovered which could affect the content, and all legal disclaimers that apply to the book series pertain.

Although reasonable efforts have been made to obtain all necessary permissions from third parties to include their copyrighted content within this article, their full citation and copyright line may not be present in this Accepted Manuscript version. Before using any content from this article, please refer to the Version of Record once published for full citation and copyright details, as permissions may be required.

Explosive sequence of La Soufrière St Vincent April 2021: insights into drivers and consequences via eruptive products

Cole P. D.¹, Barclay J.², Robertson R. E. A.³, Mitchell S.⁴, Davies B. V.², Constantinescu R.^{5,6}, Sparks R. S. J.⁴, Aspinall W.⁴ Stinton A.^{3,7},

¹School of Geography, Earth and Environmental Sciences, University of Plymouth, PL4 8AA Plymouth, United Kingdom

²School of Environmental Sciences, University of East Anglia, NR4 7TJ Norwich, United Kingdom

³University of West Indies Seismic Research Centre, St. Augustine, Trinidad & Tobago, West Indies

⁴School of Earth Sciences, University of Bristol, BS8 1RJ Bristol, United Kingdom

⁵Department of Geosciences, Environment and Society, Universite Libre de Bruxelles, Brussels, Belgium

⁶ School of Geosciences, University of South Florida, Tampa, USA

⁷Montserrat Volcano Observatory, Montserrat, Flemmings, Montserrat, West Indies

Abstract

This paper forensically reconstructs the timings, impacts and processes that drove the sequence of explosive eruptions of La Soufrière, St Vincent in April 2021 using a combination of field-based stratigraphy and textural dissection of the deposit character together with contemporary visual observations.

Explosive activity on 9th and early on 10th April involved destruction of almost all of the 2020/2021 lava dome, ~ 60% of the 1979 dome and formation of a 600 m diameter crater by 2pm UTC on 10th April. Following the initial explosion, plumes rose to altitudes of ~15 km and pyroclastic density currents (PDCs) formed by column collapse, first occurred on 10th April, only after > 24hrs of explosive activity. Dense PDCs reached the sea only in the Larikai and Roseau Valleys, and dilute PDCs were restricted to within 2.5 km of the Summit Crater rim.

The tephra fallout deposits are stratified, composed of numerous layers of both lapilli-rich and ash-rich layers, which we have grouped into at least 7 Units, based on their common characteristics (Units 1 to 7).

Volume estimates, using a range of techniques to constrain uncertainties, indicate that the bulk volume of tephra (fallout and PDC) is $1.19 \times 10^8 \text{m}^3$ +/- 20% making this a VEI 4 eruption.

Supplementary material: [video of satellite imagery sequence, Excel file of clast density data] is available at <https://doi.org/10.6084/m9.figshare.c.6474317>

1. Introduction

The island of St Vincent lies in the southern part of the Eastern Caribbean volcanic arc, and La Soufrière volcano sits at the northern end of the island (Fig 1). The volcano rises to 1204 m and 1.5 km diameter crater cuts the summit, hereafter referred to as the Summit Crater. It is the most active terrestrial volcano in the region. Having experienced four historical explosive eruptions, in 1718, 1812, 1902 and 1979, and at least one solely effusive eruption in 1971 (Robertson 2005). Radiocarbon dating has established that there were at least two prehistoric eruptions in the last 1000 years (prehistoric time is < 1700 CE in the Eastern Caribbean), one ~1580 CE, and another ~1440 CE (Cole et al. 2019).

All the explosive eruptions at La Soufrière in the last 1000 years have generated pyroclastic density currents (PDCs), however these have varied considerably in their extent. The 1902 eruption generated extensive, broadly radially distributed PDCs, resulting in the deaths of ~1500 people in settlements around the volcano (Anderson and Flett 1903). Also, the 1812 eruption generated PDCs in several valleys, particularly to the southwest, leading to fatalities (Smith, 2011). The 1979 eruption formed much smaller PDCs which, apart from in proximal regions, were confined to valleys to the west and southwest, draining the lowest part of the Summit Crater rim (Shepherd et al. 1979). Tephra fallout was extensive with all explosive eruptions, with at least the 1812, 1902 and 1979 eruptions generating ashfall in Barbados 170 km to the east (Anderson and Flett 1903, Shepherd et al. 1979). The prehistoric events in 1580 and 1440 CE were apparently larger and more intense, generating significant lapilli fallout deposits on the island prior to the onset of PDC activity (Cole et al 2019).

The April 2021 Explosive activity

Eruptive activity at La Soufrière, St Vincent restarted after a > 40 year hiatus on 27th December 2020 following a minimal period of precursory seismicity (Joseph et al. 2022, Thompson et al. 2022). Passive extrusion of a basaltic andesite lava dome then took place for ~ 3 months in the southwestern part of the Summit Crater (Stinton et al. this volume). Seismicity changed on 23 March 2021 with a short VT (volcano tectonic) earthquake swarm (226 events), a second more intense VT swarm occurred on 5th April, (476 events) followed by banded tremor on 8th April. Explosive activity started on the 9th April 2021 (Joseph et al. 2022), although this commenced with a single explosion at 12:41 UTC, the rapidity with which explosions occurred (~ hourly), together with their semi-continuous nature through the evening of the 9th April and for the following 48 hours made immediate interpretation of the nature of these explosions difficult. Much of the northern part of the island remained in darkness on 10 and 11th April, owing to the presence of extensive, semi

continuous ash plumes. Following this, explosions continued at a lower frequency until 22nd April (Joseph et al. 2022).

This paper uses a combination of field-based stratigraphy of the tephra sequence, contemporary and visual observations, along with more detailed analysis of the deposits (PDC and fallout) to reconstruct the changing nature of the explosions and their relative timing. We offer some interpretations of the critical changes that influenced explosion style and impact. The interplay between the initial overburden of the dome, the likely ingress of gassier, more buoyant magma into the conduit system, and the interactions between the vent region, accumulating Summit Crater fill deposits and the prevailing meteorological conditions all influenced the differing character of these explosions.

2. DEPOSIT CHARACTER

The Tephra sequence

Documentation of the tephra deposits was made during three field seasons. Distal products > 4 km from the Summit Crater were documented immediately following cessation of the explosive activity, between 25th April and 10th May 2021. Timed tephra sampling of measured areas was made at one location on St Vincent and two on Barbados during the explosive activity on 10 - 13th April. Two further field campaigns in early 2022 included more proximal products between 4 km and the Summit Crater rim. Overall, the tephra deposits were investigated at more than 80 locations around the island. In general, the sequence is stratified, composed of numerous layers, defined by variations in grain size and componentry. The sequence reaches >70 cm in thickness 500m southeast, and > 1 m ~ 800 m southwest of the Summit Crater. Several 'Units' were identified, from 1 to 7 from the base upwards, each Unit is composed of a number of layers with similar characteristics that we were able to recognise and correlate around the volcano (Fig 2).

Apart from in the Larikai and Roseau valleys (on the West flank) and in the proximal regions < 2.5 km from the Summit Crater rim, where PDCs occurred, deposits comprising all Units described below are considered to be fallout. PDCs were generated contemporaneously with some of these Units, and these products are described in a later section.

Below we describe the different features of the various fallout Units. Key observations are summarised in Table 1.

Unit 1 (U1)

The lowermost unit, U1, is a moderate grainsize lapilli deposit with a maximum thickness of 20 cm, 350 m southeast of the Summit Crater rim (Fig 2 and 3). At many localities it shows reverse grading, defined by the lowermost third of the unit being slightly finer grained than the upper part. This is particularly evident on the eastern side of the volcano, where the Unit is preferentially dispersed. A crude stratification, defined by small variations in grainsize of the lapilli was present, such that at least three sub-units could be identified (Fig 3 and 3a). Local horizons of hydrothermally altered fragments (up to ~20 wt%), are found close to the change in grainsize between the lower (finer-grained) and the upper (slightly coarser) parts of the unit. The contact with the overlying Unit 2 is typically defined by a fine grained laminated brown ash, a few mm thick, possibly representing a pause in deposition between Units.

Unit 2 (U2)

This Unit is a notably ash-rich, stratified deposit that reaches a maximum of 22 cm thick, 800 m east of the Summit Crater rim. The stratification is defined by the presence of numerous thin lapilli layers. In distal regions these were sometimes only a few mm thick (Fig 2 and 3). U2 shows a distinct colour change from brown (lower part) to grey (upper part).

Although generally ash-rich, at proximal locations the brown lower part of U2 is finer grained, whereas the upper part contains more abundant and coarser lapilli layers that are notably coarser than those lower in this Unit (Fig 2 and 3a). At distal locations > 4 km from the Summit Crater, these layers are typically horizons of lapilli only a clast thick, typically < 1 cm in diameter, however, notably larger lapilli of clasts 1 - 3 cm in size, both of pale vesicular scoria and dense lithologies are locally observed throughout the Unit. Up to seven individual layers were identified within the Unit, which are particularly well-defined at upwind locations (Fig 2 and 3b).

Unit 3 (U3)

This Unit is a distinctive coarse-grained, double lapilli layer couplet (L1 and L2) up to 32 cm thick, 200 m from the south-eastern Summit Crater rim, although in localities > 4 km it is typically ~2 cm thick. It forms a key marker horizon within the tephra sequence around much of the island (Fig 2 and 3).

In proximal areas, < 1km from the Summit Crater rim, the two lapilli layers are quite distinct (Fig 2 and 3c). The lowermost lapilli (L1), was up to 12 cm thick and typically contained a thin fine ash layer up to 1 cm thick, in the upper two thirds of the lapilli. Crude reverse grading is evident across the whole layer. The uppermost lapilli (L2) is a normally graded lapilli layer up to 8 cm thick. An ash layer, up to 7 cm thick, rich in accretionary lapilli separates the two lapilli layers, however in distal regions (> 4 km from the Summit Crater) this ash layer is typically < 0.5 cm thick.

This Unit forms one of the coarsest lapilli layers of the sequence with outsized lapilli up to 5 cm in diameter in distal regions that sometimes protruded through the overlying Unit 4 and into Unit 5. (Fig 2 and 3)

Unit 4 (U4)

This Unit is a single ash layer up to 12 cm thick in the most proximal locations. At more distal localities > 4 km from the Summit Crater rim this Unit is just a few mm thick. Small aggregates, including accretionary lapilli, up to 8 mm diameter are abundant in this unit (Figs 2 and 3d). Scattered coarser lapilli of both pale scoria and dense lithologies, < 5 mm diameter are also present in this Unit.

Unit 5 (U5)

The uppermost distinctive lapilli layer of the tephra sequence, this unit formed the surface carapace lapilli on the eastern (windward) side of the volcano. It is a maximum of 5 cm thick in proximal locations to the southeast, although thicknesses were difficult to estimate on the Eastern flank owing to it being the uppermost, uneven lapilli on the tephra deposit surface. Vesicular scoria lapilli and blocks are typical however, dense glassy non-vesicular clasts are also notable, giving the coarse lapilli an apparently bimodal vesicularity. In the southwestern region U5 is up to 2 cm thick and was overlain by the fine ash of Unit 6 (Fig 2 and 3)

Unit 6 (U6)

This unit is found solely on the south-western side (Leeward side) of the volcano and is formed by a number of ash layers. Collectively these form thicknesses of up to 20 cm, 2 km to the southwest of the Summit Crater, but individually these are up to 10 cm thick (Fig 1 and 2). These ash layers are notably fine grained and rich in accretionary lapilli. Individual accretionary lapilli are typically < 1 cm in size.

It is evident that some of the thickest and most abundant of these ash layers is close to the Roseau valley and upper Wallibou valleys down which PDCs travelled.

Unit 7 (U7)

Similar to U6, this Unit is found only in a few localities on the south-western side of the volcano, such as around the Dry Wallibou valley. It is formed by 3 or 4 thin, relatively fine-grained lapilli layers that are collectively up to 4 cm thick. Individual layers are 0.5-1.5 cm in thickness (Fig 2).

Pyroclastic Density currents

Pyroclastic density currents (PDCs) were associated with the explosive activity and entered several valleys draining the Summit Crater. They reached the sea in the Larikai and the Roseau valleys on the western and south-western flank of the volcano only (Fig 4a).

PDCs also extended down several of the valleys leading from the southern part of the Summit Crater rim and into the upper Wallibou valley, reaching as far as Trinity falls / Wallibou hot springs, approximately 2.5 km from the Summit Crater rim. PDCs also extended short distances (approximately 1 km) down valleys to the southeast, effectively the head of the Rabacca valley.

In proximal regions on ridges and valley sides, up to 2.5 km from the Summit Crater rim, vegetation was removed and trees were extensively felled in directions typically away from the crater (Fig 4a,5a and b). Thus, we infer that dilute, low particle concentration PDCs were responsible for this destruction and have used the presence of felled trees to map their extent (Fig 4a). Dissected deposits of the valley-filling PDCs in the Roseau and Larikai valleys, and in proximal areas on the south-eastern flank were documented (Fig 4b-e).

Larikai and Roseau valley PDC deposits

At the mouth of the Larikai Valley PDCs form a fan of deposits, 300 m wide and up to 20 m metres thick (See Fig 4b). Wood contained within the deposits is carbonised and local gas escape structures confirm a primary PDC origin for these deposits. A series of at least six massive PDC units form the Larikai fan. The lowermost unit contains regions locally enriched in coarse clasts, composed of moderately vesicular and dense glassy blocks of lava up to 3 m in diameter. Dissection of these deposits show these concentrations define convex lobate surfaces within the units. The lowermost deposits form a series of four units, without ashfall layers between them. Overlying this, three massive PDC units, interbedded with an accretionary lapilli-rich fallout layer up to 11 cm thick and a series of stratified accretionary lapilli bearing layers, collectively up to 90 cm thick (Fig 4b). A massive poorly sorted layer ~ 1 m thick, overlies the accretionary lapilli-rich fallout layer, and a stratified sequence of accretionary lapilli bearing layers collectively up to 90 cm thick occurs higher in the sequence ('S' on Fig 4b). When traced laterally these layers show notable lateral thickness variations and collectively this sequence forms large wavelength dune-bedforms. These are therefore considered to represent alternating thin PDC and fallout layers. A massive unit, up to 2 m thick, caps the sequence. Approximately 1 km up the valley the total thickness of PDC deposits reach thicknesses of up to 30 m.

Similar to the Larikai valley, dissection of deposits reveals that the Roseau valley contained several massive flow units (Fig 4c). Up to four separate units, ranging from 2 to 8 m thick individually, are

present reaching a maximum of 20 m in thickness, although more typically around 12 m. All these units contain both cauliflower vesicular and dense glassy scoria clasts up to ~50 cm in diameter. A thin 15 cm thick accretionary lapilli bearing ash fall layer is interbedded between the flow units ('A' on Fig 4c) which we correlate with the Unit 6 of the tephra fallout.

Tree branches, trunks and other vegetation contained within these deposits was generally fully carbonised, although locally some wood debris had remained uncharred.

Upper Southeastern flank deposits

On the proximal south-eastern flanks of the volcano in the region near Jacobs Well (~0.5 - 1 km from the Summit Crater rim) a series of massive, poorly sorted, valley-filling deposits up to at least 6 m thick, are observed partially filling valley depressions. Critically these massive deposits are interbedded between several tephra fallout layers, identified as Units 3, 4 and 5 (See Fig 4d). Fallout of Units 1 and 2 are present at the base of the sequence below the PDC deposits.

Vegetation and wood fragments incorporated within these massive valley-filling deposits were abraded and debarked but generally not carbonised. Nevertheless, these deposits are considered to be primary PDC deposits.

Dilute PDC deposits

Deposits formed by the dilute PDCs that caused extensive tree felling above the valley thalwegs (on slopes and ridges) were notably variable. Within 1 km of the southeast of the Summit Crater rim deposits were, < 15 cm thick, composed of fine lapilli, and typically poor in fine ash. These were identified below the U5 lapilli layer and these deposits were relatively continuous, but showed some minor local lateral thickness variations.

To the southwest of the Summit Crater rim the deposits on ridges were thicker and more extensive. A series of deposits interbedded with U3, 4 and 5 are individually 10 – 25 cm thick and up to 40 cm thick < 1 km from the Summit Crater rim and show extensive thin < 5 cm thick lenses of ash poor, fine grained lapilli within more ash rich deposits (Fig 5c). Other units are formed by variable thickness ash poor, well-sorted fine lapilli layers. Locally these deposits show crude dune bedforms and cross stratification with marked thickness variations.

The numerous trees felled by these dilute PDCs show strong abrasion, typically only on the volcano facing sides. Locally trees with trunks > 50 cm in diameter often remained standing (Fig 5 a and b). Many trees were bent over or snapped at heights of 2-3 m above the base (Fig 5a). Carbonisation of vegetation inundated by passage of these dilute PDCs was absent, although tree fern trunks

exhibited a slight blackening of their exterior. Similar lack of carbonisation of trees impacted by PDCs has been reported associated with the 18th May 1980 Mt St Helens blast PDC (Moore and Sisson 1981), the 2008 eruption of Chaiten (Swanson et al 2013, Major et al 2013) Chile, and at Kelud in Java related to the 2014 eruption (Maeno et al 2019). At Mt St Helens and Chaiten temperatures for uncharred trees were inferred to result from shortlived PDCs < 200°C.

3. CHANGING DEPOSIT CHARACTERISTICS

Grainsize analyses

Particle size analyses were undertaken on ~ 60 samples in order to characterize the grainsize of tephra and its variation through the explosion sequence. Mass fractions were acquired through manual sieving all of clasts down 125 µm, and then using a Retsch Particle Size and Shape Analyzer CAMSIZER X2 for a sub-sample of all material < 125 µm. We focussed on obtaining samples of the different Units through tephra sequences at a range of locations (Fig 6).

Cumulative grainsize distributions show a clear transition between U1 and 2, with U1 fallout deposits being notably fines-poor and U2 deposits showing a distinctly more ash-rich character (Fig 6 a). Unit 3 deposits (green lines on Fig 6a) have a varied grainsize, generated either by coarser lapilli or fine ash layers. U5 plots on the coarse side of lapilli.

The field-based subdivision of deposits into either lapilli or ash hold true in the cumulative grainsize distributions plots (Fig 6b) albeit with some overlap. Similarly, deposits identified as dilute PDCs (yellow lines on Fig 6 b) are better sorted and poorer in fine ash than other deposits.

Grainsize data through the tephra sequence show a slight coarsening upwards vertically through U1, (Sandy Bay school Md and d) - Fig 6 c) reflecting the visible reverse grading, with continued coarsening through U2. Lapilli layers of U3 or U5 form the coarsest fallout deposits of the sequence. This is corroborated by maximum clast size data (five largest clasts of both vesicular scoria and dense clasts, Figure 6c and d) . There is a general increase in maximum clast size through the sequence, with the coarsest clasts (particularly scoria) occurring either in U3 or U5.

Ash aggregates, including accretionary lapilli, were abundant from U3 onwards. Accretionary lapilli were particularly abundant on the leeward (west) side of the volcano. The presence of accretionary lapilli has impacted the grainsize distribution of deposits (Fig 6 c), and is particularly notable in ash-rich deposits on the Leeward trail where peaks at 1 phi fraction in U4 and U6 arise from ash aggregation (Fig 6c).

Component Analyses

The 2021 tephra deposits contain a wide range of components which we initially classified in the field as pale scoria (40-60% vesicles), semi vesicular (denser) scoria (20-40% vesicles), dense (sometimes glassy) clasts (<20% vesicles), hydrothermally altered fragments and free crystals. This classification was also used to broadly classify sampled fragments >1mm using the binocular microscope (Fig 7a-d).

Pale grey vesicular scoria, representing the juvenile magma, occurs in all units of the tephra sequence in varying quantities. The lowermost parts of U1 contain only 10% pale scoria (>1mm) but this increases to ~ 40 wt% of clasts in the upper part of U1. Within U2 this remains at ~ 40 wt% and in U3, lapilli layers contain up to 60 wt % pale vesicular scoria.

Dark coloured, semi- vesicular and dense clasts, (Fig 7 b and c) are most abundant in U1, forming up to 40 and 56 wt % of components > 1mm respectively. Dense clasts were present in all units forming a significant proportion (up to 40%) of U3 and U5. Hydrothermally altered clasts occurred mainly within U1 (Fig 7d). Some horizons of U1 contained up to 20 wt % hydrothermally altered fragments.

We also determined the density of sampled vesicular clasts (both pale and denser scoria) in the 16-32 mm range using the Archimedes principle to calculate the bulk density of these clasts (Fig 8). These demonstrate that there are significant variations in both mode and range of vesicularities between the Units. Clasts distinguished in the field or by binocular microscope form a continuum but generally samples classified as denser scoria have vesicularities < 30%. U1 contains a broad range of vesicularities with a mode at 25-30% vesicles. The vesicularity increases markedly to 40-45% in U2 and 45-50% vesicles in U3 and U5, which have similar vesicularity ranges.

Vesicle textures were further interrogated via quantitative analysis of BSE images for scoriaceous and semi vesicular clasts from U1, U2 and U5, and compared qualitatively with images of two clasts (semi-vesicular and scoriaceous) from U3. BSE images were acquired on a Zeiss Gemini 300 SEM at the University of East Anglia, a nested imaging strategy was applied after Shea et al., (2010) to capture the full range of vesicle sizes (See Supplementary fig 1). Key measurements including minimum pixel size are shown in Table 2. Vesicle shape and size was quantified using *Circularity* and *Roundness* parameters as defined by Liu *et al.*, (2015, the aspect ratio of the best fit ellipse and vesicle area (plotted in Fig 9 a - f). These parameters highlight key differences between U1/U2 and U5 and agree with qualitative observations of BSE images. Density plots (the representation of the relative occurrence of measurements) of vesicle area against aspect ratio (Fig. 9a – c) show that U1 and U2 have two modes in their vesicle area populations and extend to (a) smaller areas and (b) higher aspect ratios than U5, though most vesicles across all units are relatively unshaped. Density

plots of *Roundness vs Circularity* (Fig 9d – f) show more subtle differences between the bubble populations. In U5, *Circularity* and *Roundness* plot much closer to each other than U1 and U2. This indicates that for the U5 clasts analyses surface roughness exerts less of a control on bubble shape than elongation, in contrast to U1 and U2 where the increased role for surface roughness is consistent with a higher pre-existing proportion of microlites on vesiculation. BSE images of bubble textures in U1, U2 and U5 are shown below shape plots (Fig.9 g – i). Images from a semi-vesicular (Fig.9j) and a vesicular (Fig. 9.k) clast from U3 show vesicle textures intermediate between U2 and U5, with the scoriaceous clast closer to U5 and the semi-vesicular clast more closely resembling U2. A similar pattern is seen in the microlite populations of the analysed clasts (Frey *et al.*, this volume). Bubble number densities (BNDs) (corrected to remove phenocryst phases) in 2D were calculated using the analysed images, the BND of U5 is approximately half that of U1 and U2, despite having the highest vesicularity (39% in 2D). This confirms the qualitative observation that U5 has a notably larger vesicle population than either U1 or U2, but a more detailed analysis is provided in Christopher *et al.*, (this volume).

Volume of the explosive phase

In order to estimate the volume of the products of the explosive activity three different components were considered: a) tephra fallout deposits from isopach maps b) PDC deposits in valleys outside the Summit Crater and c) the intracrater fill.

Tephra fallout volume estimation from isopachs

Because there was no thickness data offshore, automated contouring over the ocean cannot be constrained to obtain closed or even partial isopach coverage. Instead, five of us ('experts') drew isopach maps for the different Units, based on the same field data available on land, but extending contours offshore with each expert providing their own best estimate, judged according to their view of the field data. In most cases, they also plotted corresponding upper and lower credible bound contours to express their assessment of appropriate uncertainties associated with the contouring, given the limited data. With this methodology, the best estimate and lower and upper contours for each Unit are taken to approximate each expert's statistical median, 5th and 95th percentile contour areas, thus allowing elementary uncertainty distributions to be quantified from each expert's judgments. (Examples of Expert 1 isopachs are shown in Figure 10).

Volumes were calculated for each experts' trio of isopach maps using the Ashcalc tool (Daggitt *et al* 2014) using the three different numerical models: Exponential (Pyle 1989), Power law (Bonadonna and Houghton 2005) and Weibull (Bonadonna and Costa 2011). We averaged the volumes

determined by these three different models, with the results corresponding to the five different experts presented in Table 3. Here we note that Figure 10 shows the central “best case” contour drawn by Expert 1. Thus, the volumes indicated for Expert 1 generally fall within the range of volumes from the other experts (see Table 3) and therefore are broadly representative when compared to the other, independently drawn alternatives.

Pooling these different judgements and uncertainties to create joint volumes was treated as an expert elicitation problem. For this purpose, the Classical Model (Cooke, 1991) combinational algorithm was adopted to aggregate deposit volumes determined from the experts’ maps and their uncertainties. These joint estimates were derived via the Classical Model pooling algorithm by equally weighting results obtained from individual experts’ maps. On this basis, piece-wise linear distributions were computed at median and 5th and 95th percentiles for the volume of each Unit. These combinations capture the experts’ uncertainty spreads jointly, thereby synthesising the deposit volume estimates into those of a single “proxy expert”, representative of the group as a whole (n.b., the details of each deposit volume joint uncertainty distribution usually differs from those indicated by isopachs drawn by any individual expert).

Next, the piece-wise linear, equal weights Unit deposit volume uncertainty distributions -- obtained from the isopach maps as described above – are stochastically sampled using the UNINET* Bayes Net software package. Summing these stochastic samplings of the deposit volume uncertainty distributions, collectively, allows an overall estimate of the total volume in all the Units to be determined from the different isopachs mapped by individual experts (Mean volumes of Units 1-3 range from 7.9 -24.2 x 10⁶ m³), with related uncertainties taken into account formally (see Table 4 for details). This uncertainty-based approach represents a more informative way of gauging quantitatively the eruption volumes derived from statistical methods. Reporting the eruption volumes with an uncertainty interval is preferred to using just ‘best estimate’ deposit volumes on their own as it can provide a clearer view of our understanding of the deposit (e.g., Constantinescu et al., 2022).

Volume of Pyroclastic density currents

The volume of pyroclastic density currents was estimated using the typical maximum thickness measured of the deposits in the different valleys. Thicknesses of PDCs in the Upper Wallibou valleys were not measured directly, therefore we assumed a thickness similar to the other nearby valleys of 10 m. We assumed box canyon type cross sections as this is the typical present day morphology of

these valleys. We obtain $\sim 17 \times 10^6 \text{ m}^3$ for the volume of the PDC deposits in the valleys outside the crater and acknowledge the considerable uncertainty in this estimate.

Intracrater tephra volume

Estimation of the volume of tephra inside the Summit Crater (see Table 5) was made by differencing of a post eruption Digital elevation model (DEM) made by photogrammetry in June 2021 with a pre-eruption DEM (Pleiades DEM). Almost complete destruction of the 2021 lava dome by the explosive activity means the absence of the 2021 lava dome from the pre-eruption topography does not significantly affect this calculation. This DEM differencing yields a volume of $43 \times 10^6 \text{ m}^3$ (uncertainties on this are $\sim \pm 20\%$, so $\pm \sim 10 \times 10^6 \text{ m}^3$).

The bulk total (non-DRE) volume of tephra is $\sim 119 \times 10^6 \text{ m}^3$ (Table 5). Lava domes form a significant contribution to the tephra deposits, we assume the 2021 lava dome had a volume of $\sim 20 \times 10^6 \text{ m}^3$ prior to the explosions and around 60% of the 1979 dome ($\sim 28 \times 10^6 \text{ m}^3$) was destroyed during the explosions. Thus, the fragmented lava domes form $\sim 40\%$ of the bulk volume of the tephra.

Therefore, $71 \times 10^6 \text{ m}^3$ of the volume might be new magma-, which converts to $42 \times 10^6 \text{ m}^3$ DRE using a 0.6 conversion based on measured tephra densities of 1500 kg m^{-3} . Here we note that the question of what constitutes “new magma” is not so straightforward as this eruption excavated and incorporated the 2020-2021 lava dome as well as incorporating new magma (see discussion below).

Comparison with other volume estimates

Our volume estimates are consistent with two other independent estimates using different kinds of data. Sparks et al. (this volume) used RSAM data and estimates of column heights from satellite data to estimate erupted volumes in each explosive event. Magma supply rates and magma volumes can then be inferred from these data. Their total DRE volume estimate is $37.8 \times 10^6 \text{ m}^3$ (90% credible interval: $[33.5 \dots 42.5] \times 10^6 \text{ m}^3$) which is very similar to the DRE derived from the isopach maps of the tephra deposits (DRE $35.5 \times 10^6 \text{ m}^3$) using a bulk volume of $59.1 \times 10^6 \text{ m}^3$ (Table 4). This apparently close agreement is somewhat misleading because there are uncertainties relating to proportions of non-juvenile clasts in the tephra deposits and excluding the very proximal deposits in the Summit Crater from the isopach volumes and the difficulty in estimating their contribution of heat to the plumes. These uncertainties would push volume estimates in the opposite directions, however, so to some extent cancel one another out. Camejo-Harry et al. (this volume) using ground deformation data estimate a volume change of $50 \times 10^6 \text{ m}^3$ in the first three days of the explosive phase of the eruption and this corresponds to the volume (DRE) of erupted magma.

4. RECONSTRUCTING THE TIMING OF THE UNITS AND THEIR ASSOCIATION WITH EXPLOSIONS

We use multiple strands of evidence to infer the timings of the Units within the explosive cycle, and hence the likely number of explosions or explosive pulses each unit represents. In turn, these timings can help us to reconstruct the impacts and important drivers of the changing explosive sequence. The evidence for these timings is given below and is also summarised in Table 6. We also show the timing of these Units graphically, overlain on real-time seismic amplitude measurement (RSAM) in Figure 11.

Re-processed GOES-16 satellite imagery that combines the IR (infrared) anomaly with ash detected in visible light ('ABI RadF ash') was used to determine the timing and distribution pattern of the explosive activity, where distinct individual explosions and matched the associated tephra (supplementary file 2). These timings correspond broadly with the seismic energy associated with each explosive pulse (expressed via RSAM, Sparks et al., this volume). Observers based on St Vincent, particularly from later on 9th April until the morning of the 11th of April, noted that individual explosive events or plumes were difficult to distinguish even during daylight hours. We have triangulated the remote sensing observations with descriptions from local observers, shared during discussion (from our first field season) or at the time of the eruption via social media, along with our field data.

U1

The initial explosion of the eruption occurred at 12:41 UTC, on 9th April and was followed by a second, smaller explosion at 18:59 UTC. Photographic documentation (Fig 12a) and satellite imagery shows that from this point onwards through the night of the 9 /10th April a near continuous pulsatory plume occurred that dispersed tephra towards the ENE. The RSAM (Real Time Seismic Amplitude Measurement) shows continuous seismicity, although a number of distinct peaks can be identified (Fig 11). To be consistent with other papers in this volume and the contemporary seismic analysis (Sparks et al., this volume) we have assigned three events to this period, with a further two more distinct explosions towards the end of the U1 sequence.

The continuous pulsatory nature of the explosive activity from 18:59 UTC on 9th April until 04:30 on 10th April is consistent with the deposit character of U1, where deposits are crudely stratified, even at relatively proximal locations. The increase in grain-size upwards (See grainsize section for more details) through U1 is associated with the latter explosions forming from higher plumes. Eyewitness

accounts from Windward residents on or close to the ENE dispersal axis describe pulse-like venting and continuous noise consistent with the fallout of lapilli-sized tephra on 9th overnight into 10th April. An isopach map shows that U1 had a north-easterly dispersal (Fig 10a). No fallout was reported in Barbados on 9th April, indicating that the plume dispersed to the north of the island supporting this north-easterly dispersal. The presence of ash on the ground at Calliaqua (south coast) at dawn on 10th April suggests that larger U1 explosions with more widespread tephra plumes began in the early hours of 10th April.

Radar imagery (Capella Space) at 14:03 UTC on 10th April showed the presence of a crater 600m in diameter inside the southwestern portion of the Summit Crater, with almost all of the 2021 dome and ~ 60% of the 1979 dome destroyed by formation of this crater. Hereafter we refer to this as the 2021 Crater.

U2

The tephra plumes generated from 09:35 UTC onwards on 10th April began to form larger more axisymmetric ABI RadF ash footprint, suggesting near island-wide dispersal, and closely spaced explosive pulses, (interval \leq 70 minutes) with a dispersal axis to the WSW. Photographic documentation also shows a particularly large asymmetrically spreading plume at 09:59 UTC (Fig 12b). Given the timing and geometry of this explosion plume we infer that this represents the start of explosive activity responsible for U2 tephra. An isopach map for this unit shows island wide ashfall occurred being dispersed generally to the WSW (Fig 10b).

U3

Observers in the Leeward areas all describe an intensification of activity during the late afternoon of the 10th of April – ‘an early night’ at Spring village (Leeward) where significant ashfall was reported between evening of 10th and 11th April (with intense lightning).

If we assume the seven layers in U2 correspond with discrete explosive events – the seventh explosion in the U2 sequence occurred at 16:20 UTC on 10th April implying that the explosion at 16:30 local time (18:30 UTC) would have been the first of the U3 tephra. However, local observations are insufficiently distinct to distinguish between these two times. RSAM data suggest that the explosion at 18:30 UTC generated a more unusual RSAM peak with longer more diffuse energy and higher frequency (Fig 11) that could be PDC formation, which is associated with this phase. This later explosion is more likely to draw comments about an ‘early night’ and is associated

with fallout in SE of the island. Thus, we suggest that the first part of the U3 sequence and the onset of PDC is associated with the 18:30 UTC explosion. The Isopach map shows a broadly axisymmetric dispersal for this unit on island with preferential dispersal to the east (Fig 10c).

We have ascribed three explosions to this Unit, the third associated with the ash of U4. Its also possible that U4 ash represents Co-PDC ashfall out settling between explosions. Atmospheric conditions at this time were wet which may explain the generation of the accretionary lapilli bearing, ash-rich deposit formed.

U5

We have assigned four of the explosions to U5, although there is considerable uncertainty about this. An increase in RSAM associated with the explosion-that-cut-the-power overnight (See Fig 1104:59 UTC 11th April), is consistent with an eruption that would have the intensity to generate some of the larger scoria, and we suggest that this represents some of the activity that formed the U5 unit.

U6

By early morning on the 11th of April most observers on the Windward (eastern side of the volcano) were reporting a clearing atmosphere and very little further ash fell, and U6 is absent here. Thus, we are confident that this is the time when it is most likely that the accretionary lapilli bearing ash layers of U6, which are abundant on the Western side of the volcano was formed from a sequence of explosions. U6 accretionary lapilli bearing ash layers are interbedded with PDC deposits in the Larikai and Roseau valleys, indicating that PDCs continued to be formed in those valleys, associated with these explosions from 10:36 UTC on 11th April.

The presence of accretionary lapilli records high moisture levels in the plumes that formed these units. As the accretionary lapilli-rich ash layers of this Unit are mainly seen in deposits on the south-west side of the volcano (Fig 10b) one possibility is that the ash layers associated with this Unit were formed as a result of PDCs entering the sea in the Larikai and Roseau valleys.

U7

Following the 11 April activity, explosions had a lower inferred column height (and a lengthening repose between explosion interval) consistent with the deposits of U7 chiefly being observed on the

Leeward side of the island (Fig 3) with the greater part of the ash column being transported by the Tropospheric trade winds.

Timing and duration of PDCs

Field evidence indicates that the first PDCs to travel out of the Summit Crater were associated with U3 explosions. Satellite imagery and eyewitness observations indicates that U3 commenced before the end of 10th April, perhaps in the later afternoon/ early evening (see table 6 and Fig 11). Partially carbonised trees washed up at Chateaubelair at midday on 11th April also support the occurrence of PDCs earlier that day or on the evening of the 10th April. Evidence also indicates that U5 activity began in the early hours of 11th April and PDCs in the proximal SE flank were clearly associated with these explosions. Radar imagery (Disaster charter imagery) acquired on 11th April 19:56 showed that PDCs had entered several valleys to the south and south-west before that time.

Two lines of field evidence clearly demonstrate that PDCs were associated with several discrete explosions, possibly over a number of days: ash fallout layers are interbedded between some PDC flow units in both the Larikai and Roseau valleys; and secondly fallout layers U3, U4 and U5 are interbedded between PDC flow units in the proximal south-eastern area. Although evidence indicates that PDCs continued to be formed associated with U6 and U7 and were probably concentrated in the Larikai and Roseau valleys.

5. DISCUSSION

The initial explosive activity between 12:36 UTC on 9th April and 9:35 UTC on 10th April resulted in the destruction of the 2021 lava coulee and ~60% of the 1979 lava dome, and formation of the 600 m wide 2021 crater that was observed in radar imagery at 14:03 UTC on 10th April. This activity formed the U1 lapilli deposit that is ash poor and rich in hydrothermally-altered, semi-vesicular and non-vesicular material. It is likely that some of these dense fragments have been sourced from these pre-existing lavas. Crude layering and reverse grading present in U1 together with an increase in grain size and abundance of vesicular scoria, testifies to the pulsatory nature and increasing intensity. Our componentry suggests an increasing proportion of primary vesiculating magma through this period. These observations are consistent with the early stages of explosive eruptions in which near surface overpressures are high, resulting in excavation of a 2021 crater and conduit system (Sparks et al. 2006).

After the initial explosive phase that formed U1 deposits and the 2021 crater, there was a pause in explosive activity for more than four hours during which a swarm of VT earthquakes occurred, with

some evidence that these became deeper with time. These coincided with rapid deflation inferred from surface deformation data (Camejo-Harry et al., this volume) and a pulse of SO₂ associated with the initial plume (Esse et al., this volume). We propose that these VTs were associated with the rapid ascent of a new pulse of gas-rich magma that resulted in the character of the deposits associated with Units 2 – 5.

Furthermore, our analysis of bubble density and shape (Fig 9) suggests that vesiculation processes leading up to U1 explosions were inhibited by the microlite-rich character of the magma at that time, as well as the work to be done excavating the 2021 crater and removing the overlying lava. We interpret the full sequence of tephra deposits in terms of a model developed for kimberlite explosive volcanism (Sparks et al. 2006) but which is more generally applicable. In this model an initially overpressured regime excavates the crater and conduit area, succeeded by a pressure-adjusted regime that includes infilling of the crater-conduit systems with tephra and clastic materials derived from further instability of the 2021 crater and conduit walls.

Juvenile magma from U1 also shows a notably lower vesicularity than that in U2 (Fig 8 and Table 2). Microtextural studies (Frey et al, this volume) show that U1 juvenile material was distinctly richer in microlites, and contained different phases, than later Units. The U1 magma was likely from a different source to those of later Units. Texturally it is the most distinctive of our erupted magmas, the groundmass is dominated by crystals with a short axis < 5 µm and aspect ratios greater than 1: 3, median vesicle area is the smallest (109 µm²) and it has the highest BND (167 bubbles/mm²).

Activity from 9:30 to 18:50 UTC on 10th April was characterised by closely spaced explosions (<1 – 2 hrs apart) and is correlated with the ash-rich U2 deposits. We attribute the change to the influence of an established crater-conduit system in which material falling back into the conduit interacts with erupting magma. Satellite imagery shows that the 2021 crater, including a tephra rim up to 40 m thick had formed from the early part of U2 activity. We envisage instability of the unconsolidated tephra rim and crater-conduit walls together with fall back of tephra into the 2021 crater and conduit led could have led to the generation of ash through fragmentation of these recycled materials. However, it also possible that the rapidity of the explosions led to a near continuous slow fallout of the ash component punctuated by coarse fallout from the explosions.

Field evidence strongly indicates that onset of the first significant PDC activity was associated with U3 activity from 21:30 UTC on 10th April. Proximal tephra sequences show no evidence of PDCs until after deposition of the ash-rich U2 tephra fallout. Distinctive U3 lapilli fallout interbedded with PDCs testifies to the onset of PDCs at this time. In addition, particularly large axisymmetric explosion

derived plumes causing early darkness in the afternoon of 10th April is coincident with vigorous explosions of U3. We suggest that processes, such as conduit widening (or perhaps when the excavation of looser tephra was more complete) are likely causes of this transition to PDC activity, this seems likely as > 24 hours of semi continuous explosive activity had already occurred. As U3 fallout deposits are some of the coarsest, most vesicular of the sequence, we rule out a decreasing gas content of the magma playing an important role in the switch to collapsing columns.

The U3 activity also marks the onset of the appearance of aggregates and accretionary lapilli within the tephra fall deposits. Accretionary lapilli and ash aggregation only need moisture-rich plumes to form. There are several sources of moisture which could have promoted ash aggregation. First, moisture-rich weather systems generating rainfall on the island associated with the explosive activity occurred from 11th April. Another origin for the moisture is from PDCs entering the sea. During the 1995-2010 activity at Soufriere Hills, Montserrat accretionary lapilli were formed at numerous times from PDCs entering the sea and generating fallout layers rich in these ash aggregates (Burns et al. 2017). Finally, it is possible that ground waters ingressed into the conduit but there is no evidence of hydrovolcanism so we think this less likely. We therefore consider that these accretionary lapilli were formed where either tephra plumes interacted with moisture-rich weather systems or where moisture-rich plumes were formed by PDCs that entered the sea.

Accretionary lapilli are abundant in numerous ash layers within the upper part of the sequence. Some of these ash layers are likely formed from elutriation of ash from PDCs, and the abundance of ash layers in sequences on the southwestern flank supports a co-PDC origin. The ash layer that occurs between the two coarse lapilli layers of U3 and the U4 ash layer are both likely to have been co-PDC ash fallout layers, occasional coarse clasts embedded within the U4 ash probably relate to continued minor explosive activity during settling of these ash layers.

The implications from the distribution and size of the scoria associated with the U5 explosions are that these were some of the largest and strongest plumes during the course of eruption. This requires some explanation as at this time the explosions had been ongoing for around 40 hours, and are close to the point at which Sparks et al., (this volume) have identified a waning stage for the eruption based on seismic energy and plume height. These scoria have a normal distribution of bulk vesicularities, and the lowest bubble number density and greatest vesicle areas (77 bubbles/mm²). With both U2 and U3 scoria showing wider distributions of vesicularities, we infer from this that U2 and U3 explosions were composed of a mixture of the initial magmas as well as driven from behind by the newer magmatic batch, a concept supported by the changing microlite populations identified

in Frey *et al.*, (this volume). We postulate that at the point of the U5 explosions the first source was exhausted and U5 explosions are only driven by the comparatively hotter (Frey *et al.*, this volume) new magmatic batch. The U6 and U7 explosions account for the slow depletion of this magma batch and increasing repose periods between explosions until insufficient momentum remained to generate explosions. It also coincides with the period of rapidly declining magma supply rate (Sparks *et al.*, this volume)

The character and temperatures of PDCs

It is evident that PDCs were generated by collapsing eruptions columns or fountains. Similar to those formed in other eruptions of this volcano (Hay 1959; Cole *et al.* 2019). Those that reached the sea at the mouths of the Larikai and Roseau valleys were by that point likely moving at low velocities, as there is no associated dilute PDC component in that region. Dilute PDCs only extended to a maximum distance of 2 km, inundating ridges to the south and west.

Field evidence also indicates that dilute PDCs in the proximal regions (< 2 km) had temperatures too low to carbonise vegetation (<250°C). Those PDCs which moved down the Larikai and Roseau valleys were hotter, with temperatures high enough to carbonise most wood fragments incorporated (probably > 300°C).

One possibility for these temperature differences is that the PDCs which reached the sea were formed from different explosions that had differing temperatures. A second possibility is that the dilute PDCs entrained significant quantities of air, enough to cool that portion of the PDCs below the carbonisation temperature of ~ 200°C, whereas the dense PDCs that moved down the valleys retained enough heat to carbonise the vegetation incorporated within them. A third explanation is that the duration of the dilute PDCs was brief, perhaps of the order of a few minutes, not long enough to result in carbonisation of the trees, whereas those incorporated in valley-confined PDCs remained engulfed in the hot deposits and were therefore carbonised.

Comparison to other eruptions at La Soufrière St Vincent and elsewhere

La Soufrière St Vincent is the most active terrestrial volcano in the Eastern Caribbean. Prior to 2021, there had been at least six explosive eruptions over the last 1000 years (Cole *et al.* 2019). It is therefore of considerable interest how the 2020/2021 eruption compares to these previous eruptions.

Our volume estimations indicate that the combined volume from the 2021 explosive eruptions was of VEI 4 magnitude. The 1979 was considered to be VEI 3, although the PDCs deposits have a

relatively similar distribution at least in the Roseau and Larikai valleys (Sigurdsson et al. 1979). Tephra fallout on island associated with the 1979 eruption is notably thinner (Brazier et al. 1982). Although no detailed isopach maps have been constructed for the 1902 eruption) the extensive, radial nature of PDCs around the volcano, and the work of Pyle et al (2018) indicate that the combined output during the 1902 eruptions on the 6-7th of May would put this eruption VEI 5 category. The 1902-03 eruptions were perhaps unique in that following the intense activity over 24 hours on the 6th-7th of May 1902 there were subsequently a further 4 further discrete explosive episodes, the last of which (in March 1903) produced basaltic scoria (Cole et al., 2019).

The 1812 eruption lasted for several days from the 27th of April to the 1st of May with a residual explosion on the 6th May (Hugh Perry Keane Accounts, quoted in Smith, 2011). From contemporary accounts the most violent phase was from the 30th April to the 1st of May and although nearby inhabitants were engulfed in darkness and pelted with 'showers of stones & earth and rocks' (Hugh Perry Keane in Smith, 2011) it is clear from these accounts that this consisted of a repetitive series of explosions. Accounts indicate that PDCs generated occurred only after several days of explosive activity that generated tephra fallout (Shepherd 1831 and contemporary Parliamentary Record). This pattern is similar to the 2021 explosive activity, where PDCs only occurred following > 24 hours of significant explosive activity. However, our preliminary geological observations indicate that these 1812 PDCs, although not as extensive as 1902, were considerably larger than those of the 2021 events, and, as yet there is no written evidence for a preceding dome-forming eruption.

Prior to both the 1902 and 1979 a lake was present in the Summit Crater and indeed for both these events hydrovolcanic activity has been invoked for the eruption mechanism of the 1979 explosions (Shepherd et al. 1979; Shepherd and Sigurdsson, 1982), and owing to abundant lithic material, for the opening phases on the 1902 eruption (Cole et al. 2019). The 2020/2021 eruption differs in that it began with three months of lava dome emplacement, and there was no evidence of hydrothermal water involvement or steam-rich plumes during the initial explosive phases. Thus, it seems the 2021 explosive eruption falls between 1979 and 1902 in terms of magnitude, but was quite similar in pattern and style to the eruption in 1812.

An important feature of the main phase of the 1902 eruption, the accounts of the 1812 eruptions and the 2021 eruption has been the presence of incessant and repetitive explosions that at some point during the eruption also generated PDCs and lahars. Our initial analysis of these deposits prior to their substantial erosion provides a unique record of subtle changes that lead to important changes in eruptive behaviour and impacts, paving the way for more detailed study. Comparison of

these within the context of the other deposits could provide insights into the critical drivers of eruptive transitions and these repetitive sequences of volcanic explosions.

Similar recent basaltic andesite eruptions include Kelud in Java, Indonesia, where a short-lived explosive eruption occurred in 2014 of VEI 4 magnitude, generating both PDCs and extensive tephra fallout (Maeno et al. 2019). Tephra fallout generated by the 2008 eruption of Chaiten, Chile despite being rhyolitic, is similar, composed of a multiple layered tephra fallout deposit formed by different phases of the eruption (Alfano et al 2011 and 2012) and associated PDCs (Major et al. 2013). Although Chaiten and Kelud generated blast-like PDCs, for which there is little evidence at La Soufriere St Vincent.

In summary, the 2021 eruptions of La Soufrière presented serious hazards to the population (~20,000) living around the volcano. Although PDCs generated were limited, in that they reached the coast only in two valleys to the west, similar to 1979, however only a slight increase in magnitude and intensity of future eruptions would result in more extensive and longer runout PDCs as happened in 1902.

Conclusions

1. Explosive activity between 9th and 22nd April 2021 resulted in a layered tephra deposit. The lowermost deposit, Unit 1 was associated with destruction of almost all of the 2021 lava dome and ~60% of the 1979 lava dome resulting in a 600m diameter 2021 crater.
2. Vesicular scoria representing the juvenile magma is present throughout the tephra sequence, but in varying quantities. Documented variations in the nature of the vesicularity is consistent with different batches of magma rising through the system in the first few days.
3. PDCs were only formed after > 24 hours of explosive activity, contemporaneous with several explosions. The switch from convecting to collapsing plumes is inferred to be related to vent processes, possibly flaring/widening. Dense, concentrated PDCs reached the sea in the Larikai and Roseau valleys only. Dilute PDCs were limited to within 2.5 km of the Summit Crater rim but were distributed across the lower crater rim from west to southeast.
4. Volume calculations indicate that the explosive phase of this eruption had a bulk volume of $1.19 \times 10^8 \text{ m}^3$ ($7.1 \times 10^7 \text{ m}^3$ DRE) +/- approximately 20% and therefore was a small VEI 4 eruption. Approximately one third of the volume of tephra is contained within the pre-existing Summit Crater forming deposits locally > 100m thick.
5. The changing style and characteristics of the tephra deposits can be attributed to changes in the ascending magma and the evolution of the conduit-crater system during the explosive

eruptions. In the first 20 hours a new explosion crater and deeper conduit formed.

Thereafter back-filling of the 2021 crater-conduit system by crater wall rock instability and recycling of tephra led to interactions of erupting magma with back-fill resulting in more ash-rich deposits and conditions for column collapse and PDC formation.

6. Although ash aggregates such as accretionary lapilli were abundant in the upper half of the tephra sequence, there is no evidence for hydrovolcanism, and we infer moisture was derived from weather systems or PDCs entering the sea.

Acknowledgements

Fieldwork and rock analysis was funded by NERC Urgency NE/W000725/1 to JB and PDC, and also by Royal Society APEX Award (grant: APX/ R1/180094) to JB. We'd like to thank Martin Mangler for discussions. RC acknowledges the support from the U.S. National Science Foundation (NSF) grant #1841928. Rodrigo Contreras Arratia for the seismic data included in Fig 11. We acknowledge the assistance of Dr Jon Stone who coordinated timed ashfall collection in Barbados. JB and PC would particularly like to thank Jenny Trumble for accommodation in April and May 2021.

References

- Alfano, F., Bonadonna, C., & Gurioli, L. 2012. Insights into eruption dynamics from textural analysis: the case of the May, 2008, Chaitén eruption. *Bulletin of Volcanology* 74 (9): 2095-2108. Doi 10.1007/s00445-012-0648-3.
- Alfano, F., Bonadonna, C., Volentik, A.C.M., Connor, C.B., Watt, S.F.L., Pyle, D.M. & Connor, L.J. 2011. Tephra stratigraphy and eruptive volume of the May, 2008, Chaitén eruption, Chile. *Bulletin of Volcanology* 73 (5): 613-630.
- Anderson, T., & Flett, J.S. 1903. Report on the eruptions of the La Soufrière in St. Vincent, in 1902, and on a visit to Montagne Pelée in Martinique, part I. *Phil. Trans. R. Soc. A* 200, 353–553.
- Bonadonna, C. & Houghton, B.F. 2005. Total grain-size distribution and volume of tephra-fall deposits *Bulletin of Volcanology*, 67 (2005), pp. 441-456
- Bonadonna, C., & Costa, A. 2013. Plume height, volume, and classification of explosive volcanic eruptions based on the Weibull function. *Bull Volcanol* 75:1–19
- Brazier, S., Davis, A.N., Sigurdsson, H. & Sparks, R.S.J. 1982. Fall-out and deposition of volcanic ash during the 1979 explosive eruption of the Soufriere of St. Vincent. *J. Volcanol. Geotherm. Res.*, 14 (1982), pp. 335-359
- Burns, FA., Bonadonna, C., Pioli, L., Cole, P.D. & Stinton, A. 2017. Ash aggregation during the 11 February 2010 partial dome collapse of the Soufrière Hills volcano, Montserrat. *J Volcanol Geotherm Res* 335:92–112.
- Camejo- Harry, M., Pascal, K., Ryan G et al. This Volume. Pre and Syn deformation associated with the La Soufriere volcanic eruption of 2020-21
- Christopher, T., Frey, H., Mourne, S., Manon, M., Contreras, R., Barclay, J., Davies, B.V., Joseph, E.P., Robertson, R.E.A., Henry, L. & Howe, T. (This volume.) Insights into the dynamics of the (2020-2021) La Soufriere eruption revealed from vesicle size distribution and degassing studies.
- Cole, P.D., Robertson, R.A.E., Fedele, L. & Scarpati, C. 2019. Explosive activity of the last 1000 years at La Soufrière, St Vincent, Lesser Antilles. *J. Volcanol. Geotherm. Res.*, 371 (2019), pp. 86-100.

Constantinescu, R., White, J. T., Connor, C. B., Hopulele-Gligor, A., Charbonnier, S., Thouret, J.-C., et al. 2022. Uncertainty Quantification of Eruption Source Parameters Estimated From Tephra Fall Deposits. *Geophysical Research Letters*, 49(6), e2021GL097425.
<https://agupubs.onlinelibrary.wiley.com/doi/abs/10.1029/2021GL097425>

Cooke R. M. 1991. *Experts in Uncertainty*. New York, Oxford University Press; 321 pp.

Daggitt, M.L., Mather, T.A., Pyle, D.M. & Page, S. 2014. AshCalc—a new tool for the comparison of the exponential, power-law and Weibull models of tephra deposition. *J. Appl. Volcanol.* 3 (1), 7.
<http://dx.doi.org/10.1186/2191-5040-3-7>

Esse, B., Burton, M., Hayer, C., Contreras-Arratia, R., Christopher, T., Joseph, E.P., Varnam, M. & Johnson, C. This Volume. SO₂ emissions during the 2021 eruption of La Soufrière St. Vincent, revealed with back-trajectory analysis of TROPOMI imagery.

Frey, H., Manon, M., Barclay, J., Davies, B.V., Walters, S., Cole, P.D., Christopher, T. & Joseph, E. (This volume) Petrology of the explosive deposits from the April 2021 eruption of La Soufrière volcano, St Vincent: a time-series analysis of microlites.

Hay, R.L. 1959. Formation of the Crystal-rich Glowing Avalanche Deposits of St. Vincent, B.W.I. *J. Geol.* 67, 540–562.

Joseph, E.P., Camejo-Harry, M., Christopher, T. *et al.* 2022. Responding to eruptive transitions during the 2020–2021 eruption of La Soufrière volcano, St. Vincent. *Nat Commun* 13, 4129 (2022).
<https://doi.org/10.1038/s41467-022-31901-4>.

Lange, R. & Carmichael, I.A.E. 1987. Densities of Na₂O-K₂O-CaO-MgO-FeO-Fe₂O₃-Al₂O₃-TiO₂ SiO₂ liquids: New measurements and derived partial molar properties. *Geochimica et Cosmochimica Acta.* 51/11, 2931-2946

Liu, E.J., Cashman, K.V. & Rust, A.C. 2015. Optimising shape analysis to quantify volcanic ash morphology. *GeoResJ* 8, 14-30

Maeno, F., Nakada, S., Yoshimoto, M., Shimano, T., Hokanish, N., Zaennudin, A. & Iguchi, M. 2019. A sequence of a plinian eruption preceded by dome destruction at Kelud volcano, Indonesia, on February 13, 2014, revealed from tephra fallout and pyroclastic density current deposits. *Journal of Volcanology and Geothermal Research*, 382, 24-41.

- Major, J.J., Person, T.C., Hoblitt, R.P. & Moreno, H. 2013. Pyroclastic density currents associated with the 2008–2009 eruption of Chaiten Volcano (Chile): Forest disturbances, deposits and dynamics. *Andean Geology*, **40**, 324–358.
- Pyle, D.M. 1989. The thickness, volume and grainsize of tephra fall deposits. *Bull Volcanol* 51:1–15
- Robertson, R.E.A., Barclay, J., Joseph, E.P. & Sparks, R.S.J., This Volume An overview of the eruption of La Soufriere Volcano, St. Vincent 2020 to 2021.
- Shea, T., Houghton, B.F., Gurioli, L., Cashman, K.V., Hammer, J.E. & Hobden, B.J. 2010. Textural studies of vesicles in volcanic rocks: an integrated methodology. *J Volcanol Geotherm Res*;190(3-4):271–89
- Shepherd, C. 1831. *An Historical Account of the Island of Saint Vincent*. Nicol, London (216 pp.).
- Shepherd, J.B., Aspinall, W.P., Rowley, K.C., Pereira, J., Sigurdsson, H., Fiske, R.S. & Tomblin, J.F. 1979. The eruption of Soufriere volcano, St. Vincent, April–June 1979. *Nature*, **282**, 24–28.
- Shepherd, J.B. & Sigurdsson, H. 1982. Mechanism of the 1979 explosive eruption of Soufrière volcano, St. Vincent. *J Volcanol Geotherm Res* 13:119–130
- Smith, S.D. 2011. Volcanic hazard in a slave society: the 1812 eruption of Mount Soufriere in St Vincent. *Journal of Historical Geography*, **37**, 55–67.
- Sparks, R.S.J., Aspinall, W., Barclay, J., Renfrew, I. & Stewart R. This volume. Analysis of magma flux and eruption intensity during the explosive activity at Soufrière St Vincent.
- Sparks, R.S.J., Baker, L., Brown, R.J., Field, M., Schumacher, J., Stripp, G. & Walters, A. L. 2006. Dynamical constraints of Kimberlite Volcanism. *Journal of Volcanology and Geothermal Research* 155, 18–48.
- Stinton, A., Sparks, R.S.J., Huppert, H.E. This volume. Analysis of magma rheology from lava spreading and explosive activity during the 2020–2021 eruption of the Soufrière St Vincent with implications for eruption dynamics.
- Swanson, F. J., Jones, J. A., Crisafulli, C. M., & Lara, A. 2013. Effects of volcanic and hydrologic processes on forest vegetation: Chaitén Volcano, Chile. *Andean Geology*, **40**(2), 359–391.1
- Thompson, J.O., Contreras Arratia, R., Befus, K.S., Ramsey, M.J. 2002. Thermal and seismic precursors to the explosive eruption at La Soufrière Volcano, St. Vincent in April 2022. *J Volcanol Geotherm Res* <https://doi.org/10.1016/j.epsl.2022.117621>

Figure Captions

Fig 1 The island of St Vincent and location of La Soufriere volcano on the island. Inset are the islands of the Eastern Caribbean arc. The area shaded red represents the volcanic edifice.

Fig 2 Measured sections through the 2021 tephra sequence Leeward sections (top) and Windward locations (bottom).

Fig 3 – Tephra sequence at a) Owia (5 km NE) scale in cm divisions, b) Dry Wallibou mouth (4.5 km SW of Summit Crater rim), c) River Bed 1.8 km SE, Sequence is 30 cm thick in total. d) Tephra fallout sequence at 'The Bench' 1.2 km SE of Summit Crater rim, sequence is a total of 45 cm thick. e) Sequence at Loc 38, Dark View falls 6 km SW of Summit Crater rim. Sequence is 3.8 cm thick. Scale is in 1 cm intervals. f) Accretionary lapilli in Unit 4 at Jacobs well (700 m SE of Summit Crater rim). Coin is 2cm across.

Fig 4 a) Map showing extent of PDCs, from fieldwork and satellite imagery. Red =dense valley filling PDCs. Pink = dilute PDC; PDC deposits. Yellow dots are sections shown in b-f; b) in the Larikai, c) Roseau, d) section at Jacobs well showing PDCs interbedded with fallout layers, e) Upper SE flank valley (looking South from Jacobs Well) f) Several PDC flow units interbedded between with fallout layers at Jacobs well (Upper SE flank shown in a) and d)

Fig 5 a) Tree felling ~1km SW of the Summit Crater rim on the Leeward trail. PDCs moved from left to right. Note several trees are broken 2-3 m above their base. b) Detail of trees impacted by PDCs in same region as 'a'. PDCs moved from right to left obliquely into the plane of the photograph. Note-abrasion of trees on volcano facing (RHS) side and absence of charring of trees. c) Deposits of dilute PDCs in a similar region to a) showing strong lateral thickness variations and crude cross-bedding Current direction is from left to right. Spade handle rests on U2. Pen rests on lowermost PDC deposits and is 14 cm long.

Fig 6 a) Cumulative grainsize distributions for the different units. U1 and U2 are shown as areas. Units 3 to 5 are depicted as lines for individual grainsize analyses b) cumulative grainsize distributions of the different lithofacies Lapilli and Ash layers shown as shaded areas. PDCs (dilute and concentrated) are plotted as lines of individual grainsizes analyses. Grainsize histograms and statistics through two sequences C) Windward: Mahan ridge and Sandy bay d) Proximal – Jacobs well (700 m SE). Closed symbols on Max clast sizes are dense clasts, open symbols= vesicular scoria.

Fig 7 a-d SEM images of component types a) dense b) semi vesicular c) vesicular scoria d) hydrothermally altered. e) Variations in component types > 1mm through three sequences of 2021 tephra on the Eastern (Windward) side of the volcano.

Fig 8 Vesicularity variations in juvenile clasts 16 - 32 mm in four different Units. Clast bulk densities were calculated using the Archimedes principle after Shea et al., 2010 and converted to vesicularity using a DRE value of 2.79 g/cm³ – as calculated using whole rock (XRF) data and the method of Lange and Carmichael (1987) In brackets, n = number of clasts analysed from each unit. Pie charts show the proportion of field classified vesicular and semi-vesicular clasts in the different measured vesicularity ranges.

Figure 9: Density plots of bubble shape and size from Units 1, 2 and 5 (A – F), dashed red line marks boundary at which roundness = circularity. Backscattered electron images showing changing bubble textures between Units 1, 2 and 5 (G – I) and Unit 3 (J and K). SV = clast categorised as semi-vesicular, S = clast categorised as scoriaceous. Numbers in brackets refer to 3D bulk vesicularities acquired using the Archimedes method following Shea *et al.*, (2010). *Circularity* is sensitive to deviations from a perfect circle via either surface roughness (e.g., protrusions caused by crystal interference or preservation of coalescence features), or elongation. In contrast, *Roundness* is a measure is less sensitive to protrusions on vesicle walls (Liu *et al.*, 2015). If elongation is the dominant factor, lower values of *Circularity* will be approximately equal to *Roundness* (Liu *et al.*, 2015)

Fig 10 Hand-drawn isopach maps for Expert 1 for a) U1, b) U2, c) U3, d) U4-7, e) total tephra thickness and f) interpreted distal thickness including Barbados island. Thicknesses values are in millimetres.

Fig 11 Timeline showing Real time seismic amplitude (RSAM) for (a) the whole explosive phase and (b) a detailed of RSAM and seismic frequency spectra for the first 100 hours of explosive activity. Our interpretation of the timing of the different Units (see also table 6) is superimposed on this, start times of each Unit given in Local time and UTC in parentheses. U4 is not shown simply owing to space issues.

Fig 12 a) Tephra plume at 5:15 LT (21:15 UTC) on 9th April 2021 viewed from boat just north of Kingstown approximately 19 km southwest of the volcano. Photo credit: Kai Best b) Large axisymmetric spreading plume at 5:59 LT (09:59 UTC) viewed from nr Calliaqua, close to the southernmost point of the island, 22.5 km south of the volcano. This plume likely corresponds to the start of the Unit 2 phase. Photo Credit: Jenny Trumble

Table Captions

Table 1 Summary of key features of different Units identified. N.G=normal grading. R.G. = reverse grading. S= vesicular scoria, SV= semi vesicular, D= Dense, H = hydrothermal

Table 2: Key measurements from 2D image analysis of vesicles and micro/phenocryst phases for Units 1, 2 and 5.

Table 3 Bulk volumes of the different Units calculated from isopach maps. Volumes in millions of cubic metres (to the nearest million). 'Best Case' = in bold, 95 and 5% estimates in parentheses

Table 4 Results of UNINET stochastic sampling of the EqWt Unit bulk volume piece-wise linear uncertainty distributions from EXCALIBUR. Volumes are 10^6m^3

Table 5 Bulk volumes of the different components of the explosive activity.

Table 6: (1) Explosion number – explosion assignment from Robertson et al., this volume (2) Seismic (RSAM data) to define onset on explosions and durations of RSAM signal. Data used here are RSAM Spike determinations by Sparks et al., this volume but see also Fig ?. (3) Times used here are derived from satellite data as described in Sparks et al., (this volume). Dark grey shading indicated discrete explosions less than two hours apart, light grey from 2-4 hours apart. Thick black line indicates high degree of certainty on boundary timing, lighter grey lines indicate lower degrees of certainty.

Unit	Max thickness (location)	Comments/features	Accretionary lapilli	Components
U1	20 cm (700m SE)	Crudely stratified, moderate GS lapilli (R.G.) Horizons rich in hydrothermally altered clasts	No	S ~10% at base, to 40% at top. Rich in SV clasts, H-rich horizons
U2	20 cm (700m SE)	Ash-rich, up to seven individual layers, Coarser lapilli toward top of unit	No	S ~40-50 wt % clasts
U3	31 cm (600m SE)	Double lapilli, (upper N.G.). Ash layer between lapilli	Yes	S clasts up to 60 wt %)
U4	8 cm (700m SE)	Single ash layer, some diffuse/ scattered lapilli	Yes, abundant	Sparse coarse clasts, mostly D and S.
U5	6 cm (700m SE)	Coarse lapilli, uppermost deposit to East	No	Rich in S, glassy D clasts also prominent
U6	10 cm (2 km SW)	several ash-rich layers	Yes, abundant	
U7	5 cm (4 km SW)	Thin fine grained ash and lapilli	Yes	

Table 1

	UNIT 1	UNIT 2	UNIT 5
Total area analysed (cm²)	2.19	1.55	1.65
% phenocrysts/microcrysts	24.4	22.6	18
% vesicularity	10	16	32
% vesicularity (crystal free)	27	26	39
No. analysed	32914	22816	10399
Crystal corrected area (mm²)	197	131	135
2D BND (per mm²)	167	174	77
Average vesicle area (μm²)	537	916	4358
Median vesicle area (μm²)	109	121	252
Min vesicle area*	3.78	3.76	2.93
Max vesicle area (mm²)	0.85	2.80	2.55
Average Elongation	0.3	0.3	0.29
Median Elongation	0.29	0.29	0.28
Pixel size (μm²)	0.66	0.86	0.76

- Constrained by minimum pixel size

Table 2

	Expert 1	Expert 2	Expert 3	Expert 4	Expert 5
Unit 1	15 (12,22)	11 (5,14)	15 (8,20)	18 (14,57)	10
Unit 2	19 (16,29)	15 (12, 16)	16 (12,18)	28 (18, 53)	24
Unit 3	6 (4,12)	5 (4,6)	6 (4,7)	9 (7,16)	-
Unit 4-7	15 (13,18)	12 (11,17)	8 (5,12)		
Total Thickness (From whole tephra thickness isopach)	44 (35,98)	37 (24,82)	31 (29,90)	44 (30,99)	74

Table 3

	5%ile	Median	95%ile	Mean	+/- StDev
Unit 1	4.6	14.5	51.2	21.6	+/- 15.3
Unit 2	12.2	17.2	47.1	24.2	+/- 12.5
Unit 3	3.8	6.0	15.1	7.9	+/- 3.7
Units 4-7	5.1	12.1	17.7	11.8	+/- 4.0
Summed Units	37.2	63.3	102.4	65.4	+/- 20.4
Total isopach map volume	25.6	42.3	98.0	52.7	+/- 24.3
Mean of Summed and Total				59.1	

Table 4

	Volume (x10⁶m³) to nearest million
Tephra fallout from isopachs	59 +/- 20
PDC deposits (in valleys outside the Summit Crater)	
Larikai	(6) +/-1.5
Roseau	(4) +/- 1
Upper Wallibou (3 valleys)	(6) +/-1.5
Upper South East flank (upper Rabacca)	(1) +/-0.25
	17 +/-3.5
Intracrater fill (DEM differencing)	43 +/- 10
Total bulk volume	119 +/-24

Table 5

Event # ⁽¹⁾	Day (April 2021)	RSAM Spike Time ⁽²⁾ (UTC)	Spike Duration (minutes)	Plume emergence ⁽³⁾ (UTC)	Unit	Visual/Stratigraphic observations and correlation with other geophysical datasets
1	9 th	12.41	11	12.50	U1	Distinctive explosion and plume, widely observed
2,3,4	9 th	18.59		19.00 (start)	U1	Deposit lapilli-rich/ash poor on island with slight coarsening upwards in sequence but individual pulses difficult to differentiate until last 2 explosions shown here. Following the initial pulse at 19:00 RadiF ash imagery shows near continuous pulsatory plume dispersed ENE, with some distinct pulses towards end of sequence consistent with RSAM spikes at 06:37 and 07:24 UTC.
					U1	
					U1	
	10 th			04:30 (End)	U1	
5	10 th	06:37	11		U1	
6	10 th	07:24	3	07:50	U1	Minor (ash) fallout in SE. island between midnight and 05:30 (09:30 UTC) inferred to be from last two explosions.
7	10 th	09.35	23	09.50	U2	Begins with distinct plume seen in SE island at dawn (05:35 LT, 09:35 UTC), with visible fallout. Axisymmetric plume in RadiF. Plume travels ESE. Minor ashfall begun across Barbados mid-morning, then intensifies, ashfall in Kingstown during day. Boundary uncertainty: Distinctive ash-rich deposits but with 7 discrete coarse pulses evident in medial locations (six explosions here)
8	10 th	10.47	8	11.00	U2	
9	10 th	12.02	12	12.10	U2	
10	10 th	12.54	13	13.00	U2	
11	10 th	14.27	14	14.40	U2	
12	10 th	16.20	23	16.30	U2	
13	10 th	18.30	13	18.50	U3	Distinctive distal expression as coarse lapilli couplet separated by fine ash. Proximal localities have fallout separated by PDC (and co-PDC ash). Distinctive RSAM peak consistent with the first PDC generation at 18:30 (consistent with proximal stratigraphy). Ash fallout in S. Leeward begins at this time. N. Leeward Observers describe 'an early night' around this time. Some rain in S. Island. Windward observers describe diminishing continuity or intensity of activity.
14	10 th	21.20	19	21.30	U3	
15	10 th	23.02	20	23.10	U4	Ash-rich layer with some coarser lapilli. Although U4 could be predominantly from PDC fallout, distributed across island. Boundary uncertainty: lower peak energy (RSAM) explosions could implying PDC or lower intensity ash generation
16	11 th	00.51	21	01.00	U5	Coarse scoria-rich deposits. Prominent in deposits

17	11 th	02.44	16	02.50	U5	across island, forming carapace on Windward sequences. 3 rd Explosion in this sequence cuts power across the island. Early morning rain in Barbados, combined with continued ash fall. Boundary Uncertainty: nature of U5 deposit (large scoria lodged in finer ash) makes precise no. of explosions harder to determine. Daylight visual observations more consistent with U6 explosions.
18	11 th	04.59	11	05.10	U5	
19	11 th	07.55	13	08.10	?U5	
20	11 th	10.36	13	10.50	U6	Number of fine-grained ash layers, rich in accretionary lapilli. Limited to Western flanks of volcano. PDC generation continues at this time. Eruption columns predominantly carried to Leeward in lower atmospheric winds from this time (below windshear). Rainfall on Windward side of island (lahars) – little further ash deposition on this side of island & ‘clearing air’ during morning. Steaming in Rabacca reported at this point.
21	11 th	13.24	22	13.40	U6	
22	11 th	18.11	11	18.20	U6	
23	11 th	20.22	12	20.20	U6	
24	12 th	00.39	18	00.50	U7?	Majority of this sequence is manifest in fine indistinct ash sequence of U7 (when present at all – only found proximal to volcano). N. Leeward observers report no ash by 13 th April. PDCs still observed. Rainfall continues on 12 th and 13 th April. Ashfall in Barbados now negligible. We infer that there would be almost no fallout visible in our sequence from the last three explosions.
25	12 th	07.59	20	08.10	U7 ?	
26	12 th	20.53	24	21.30	U7?	
27	13 th	10.23	24	10.40	U7?	
28	14 th	02.27	17	02.40	U7 ?	
29	14 th	15.31	10	15.40	U7?	
30	16 th	10.16	5	10.50	-	
31	18 th	20.49	10	21.00	-	
32	22 nd	15.09	9		-	

Table 6

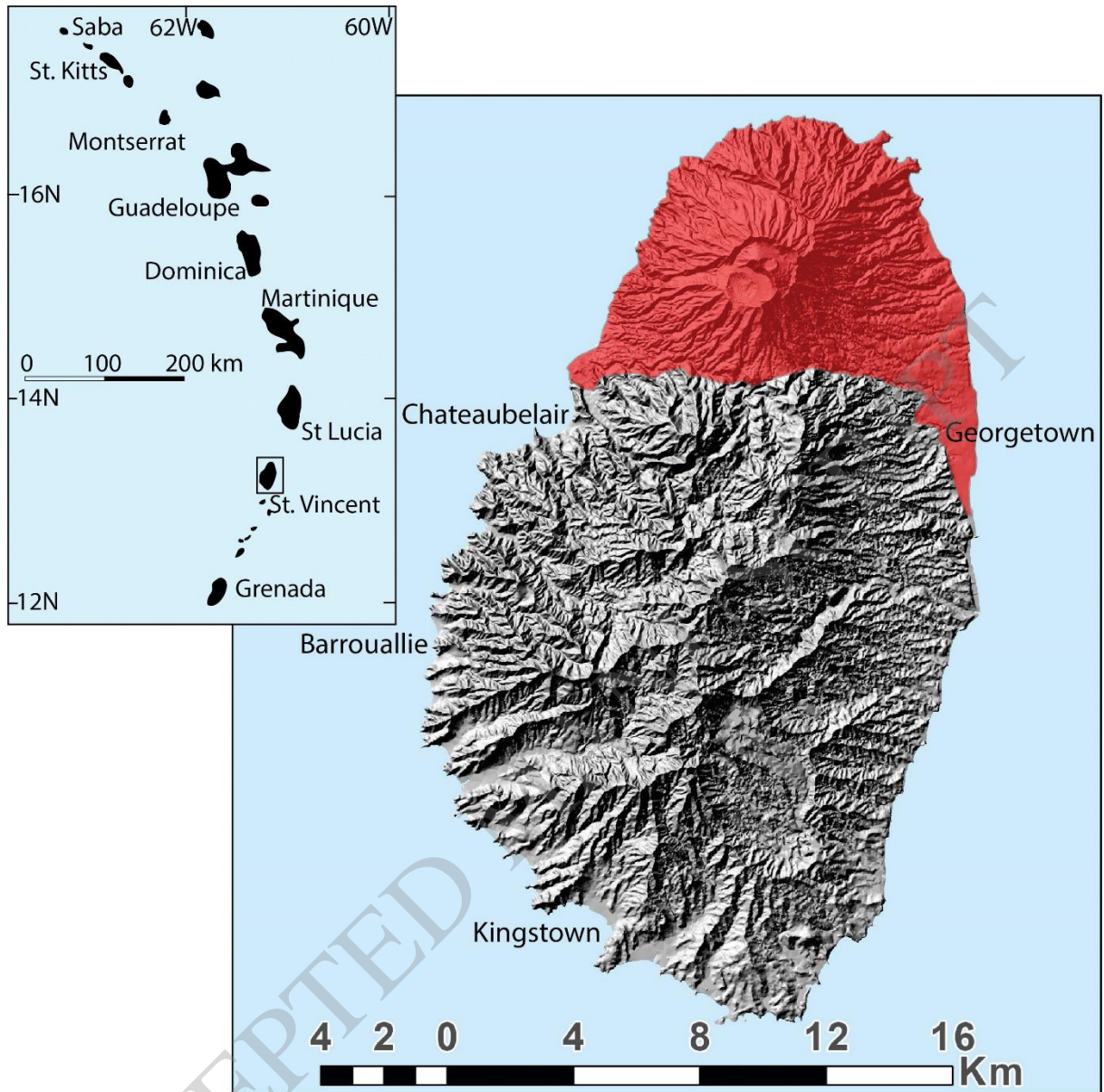


Figure 1

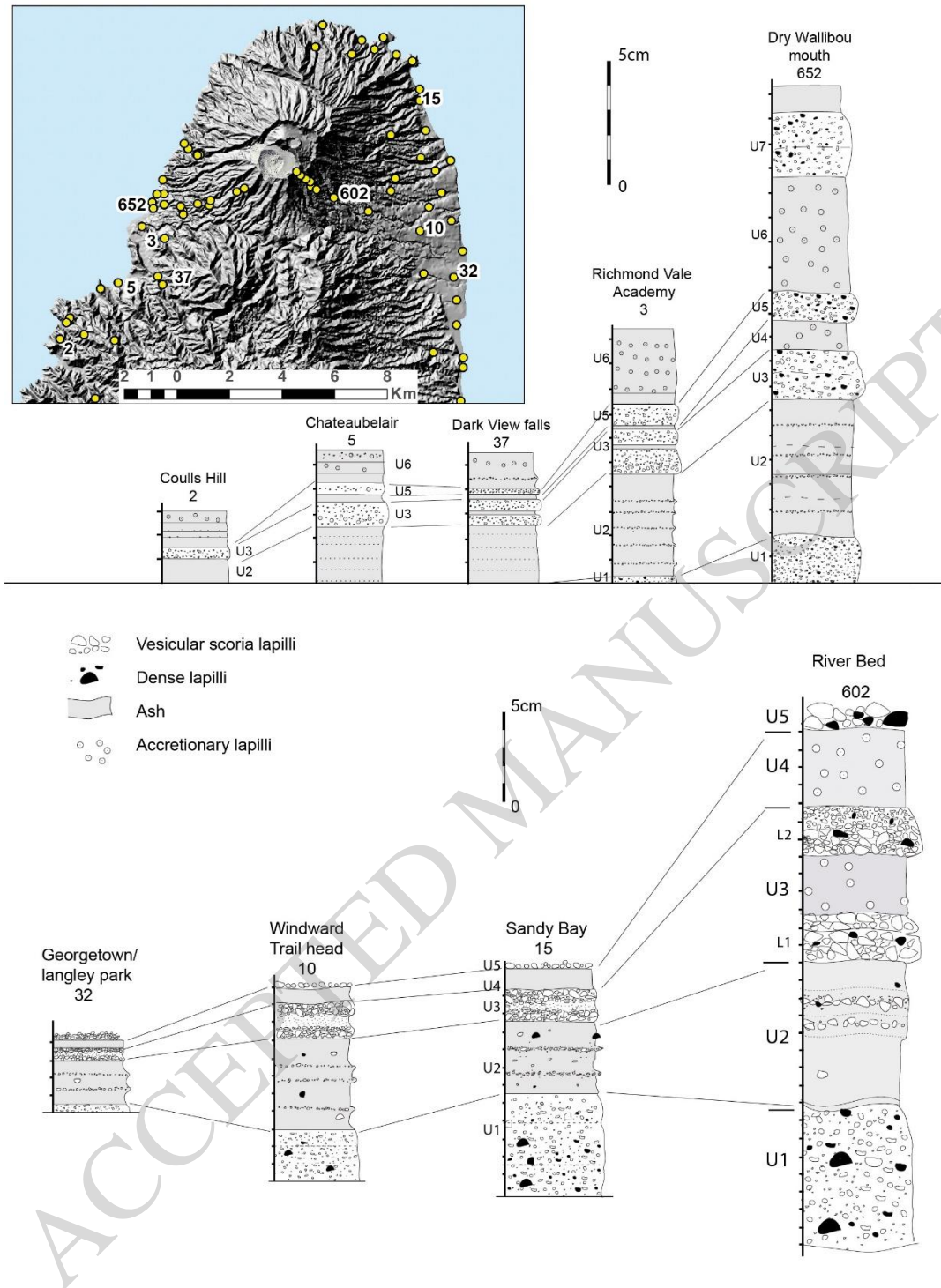


Figure 2

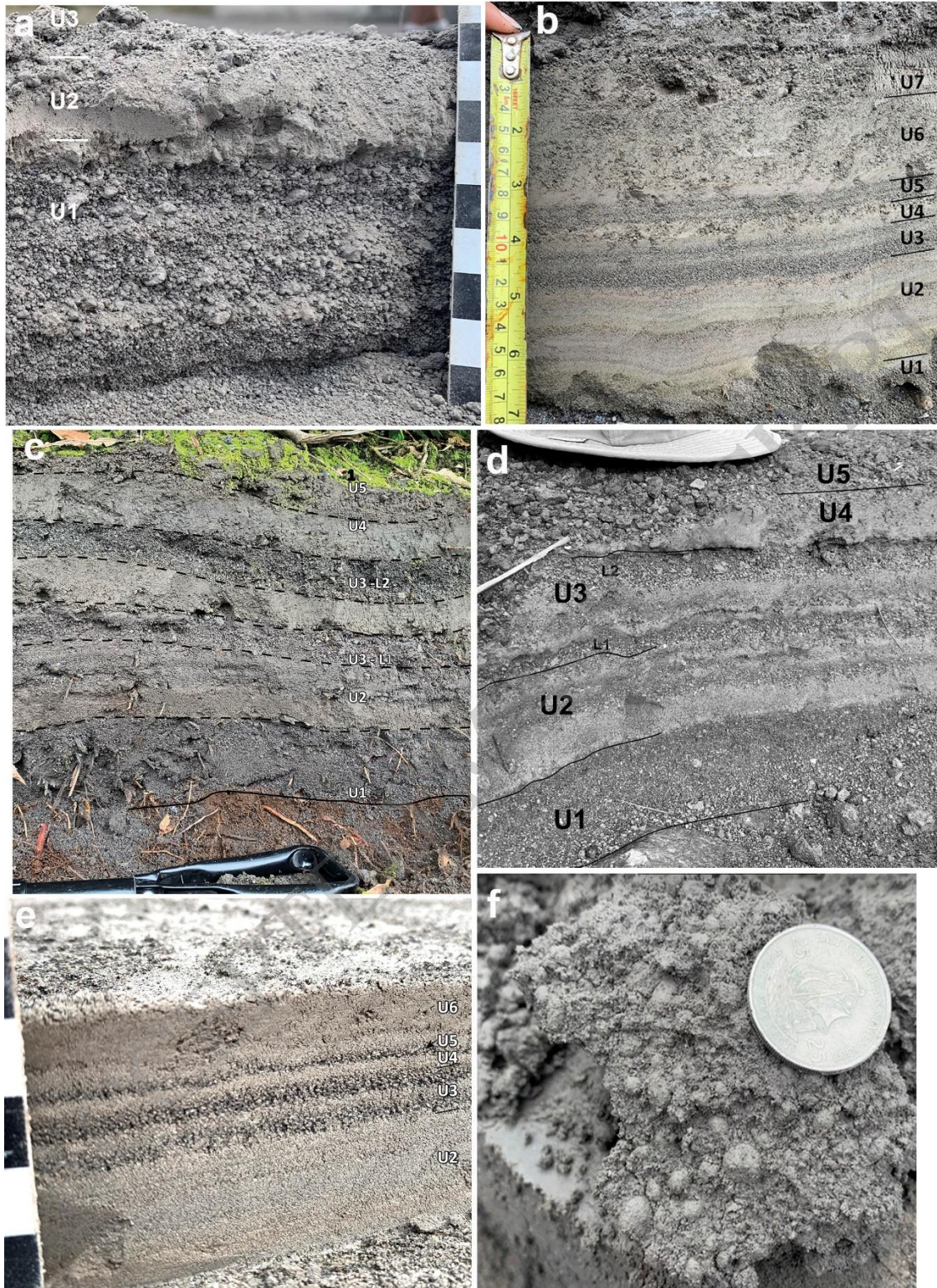


Figure 3

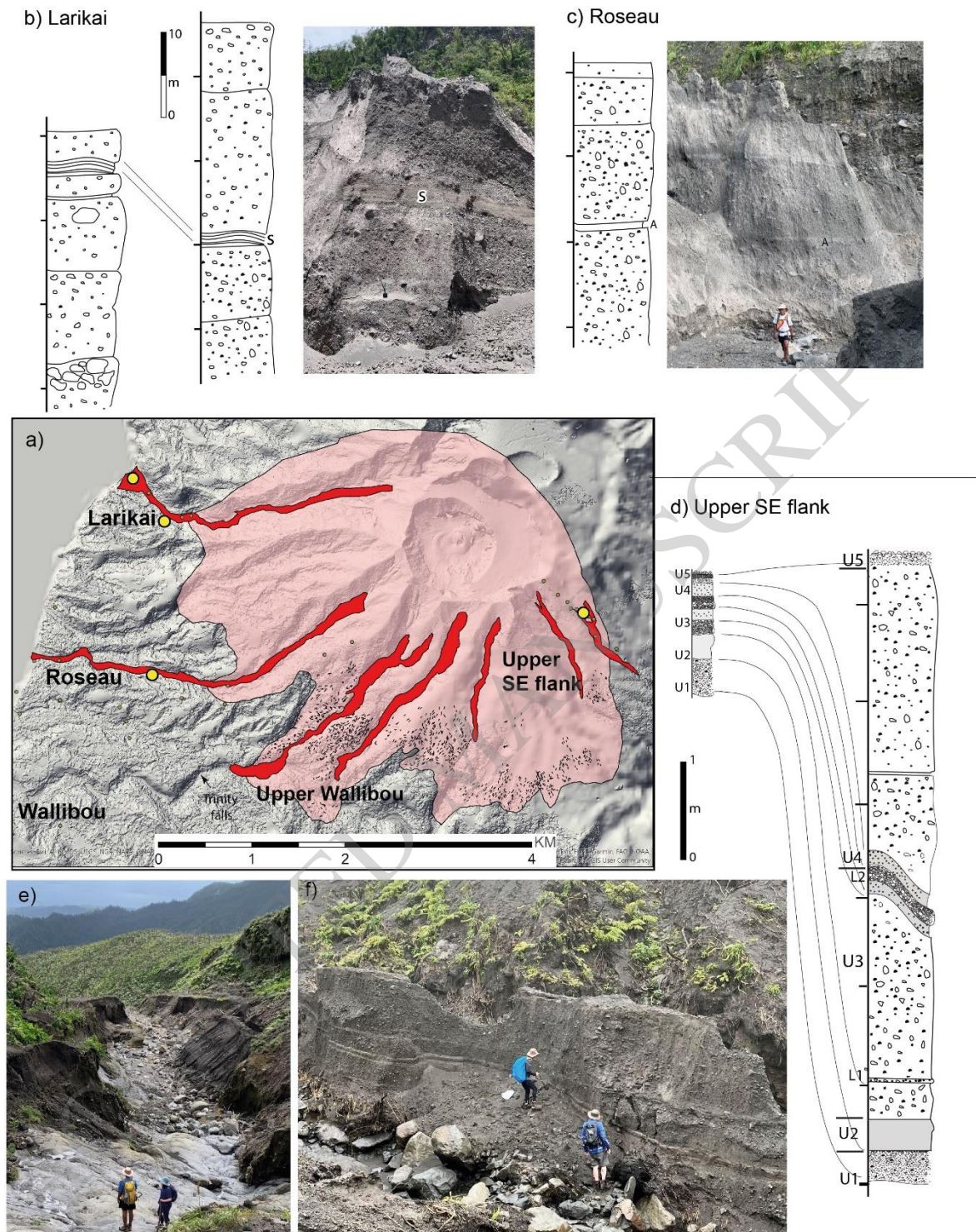


Figure 4



Figure 5

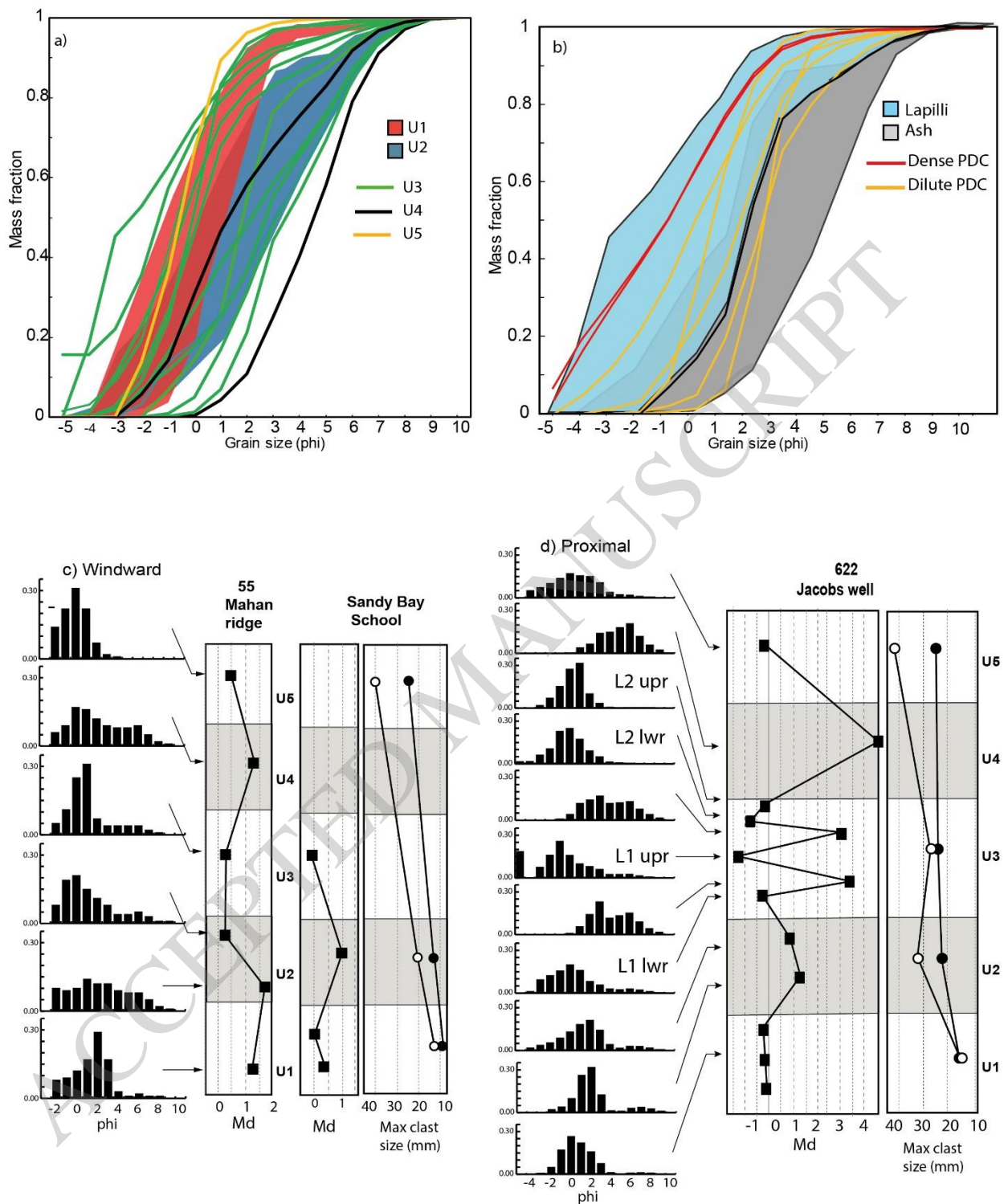


Figure 6

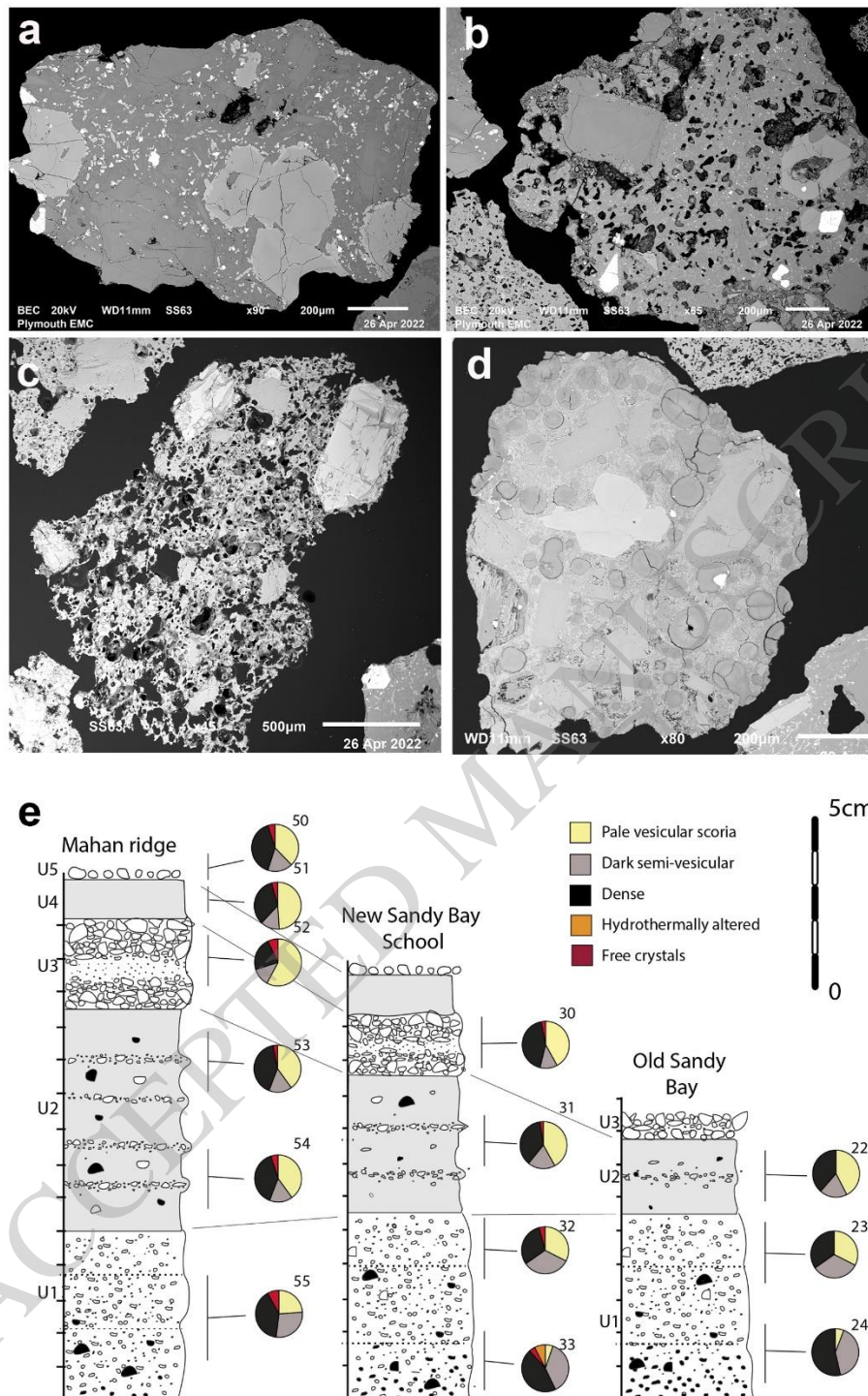


Figure 7

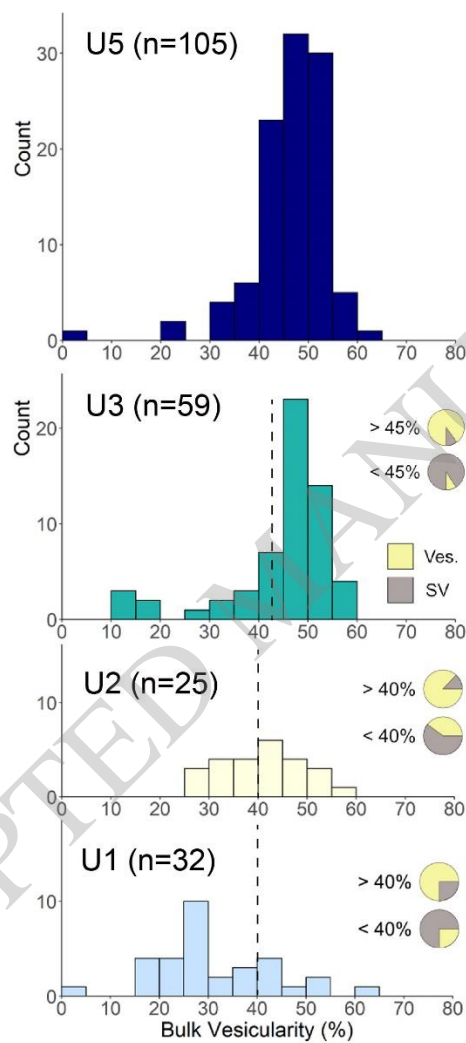


Figure 8

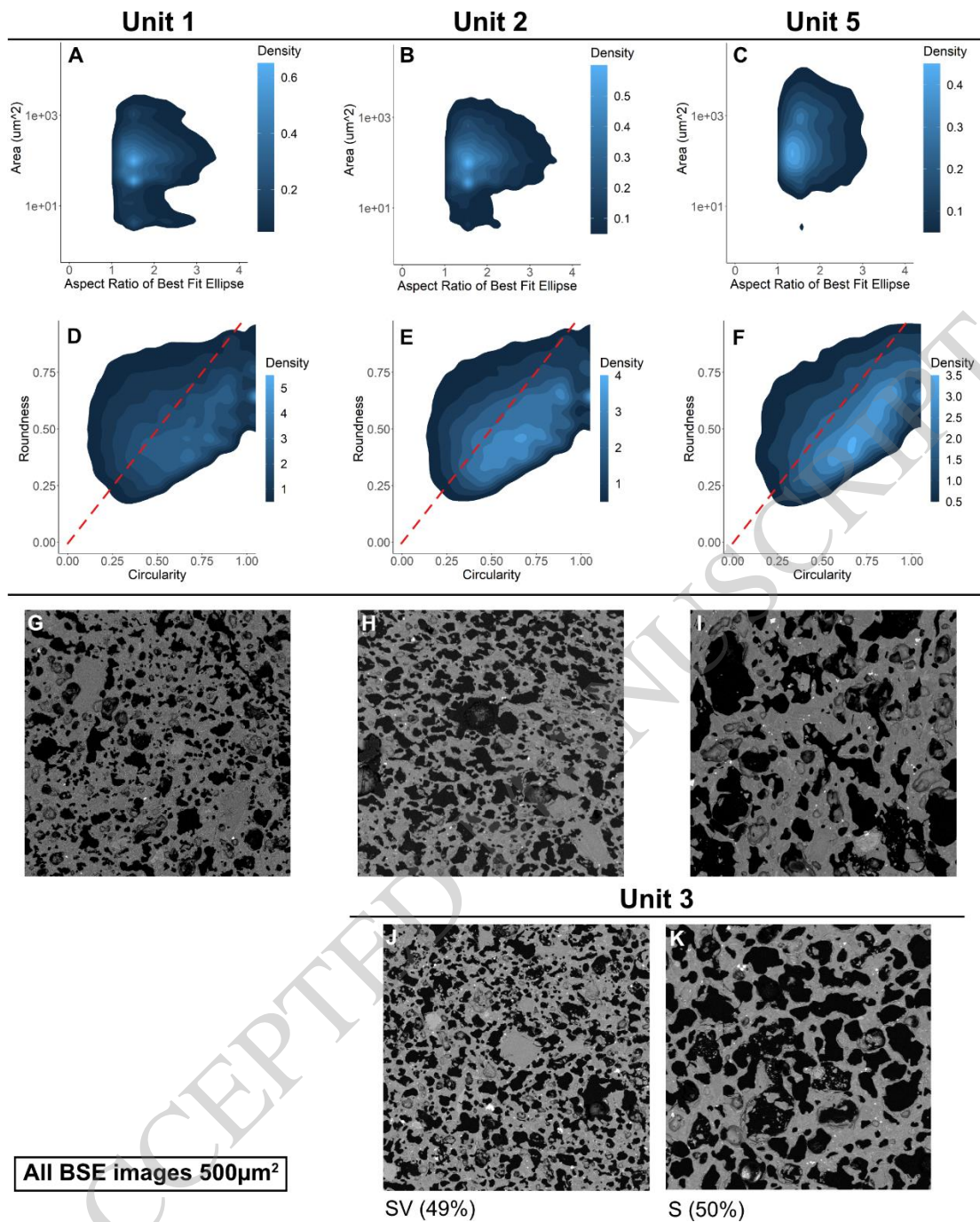


Figure 9

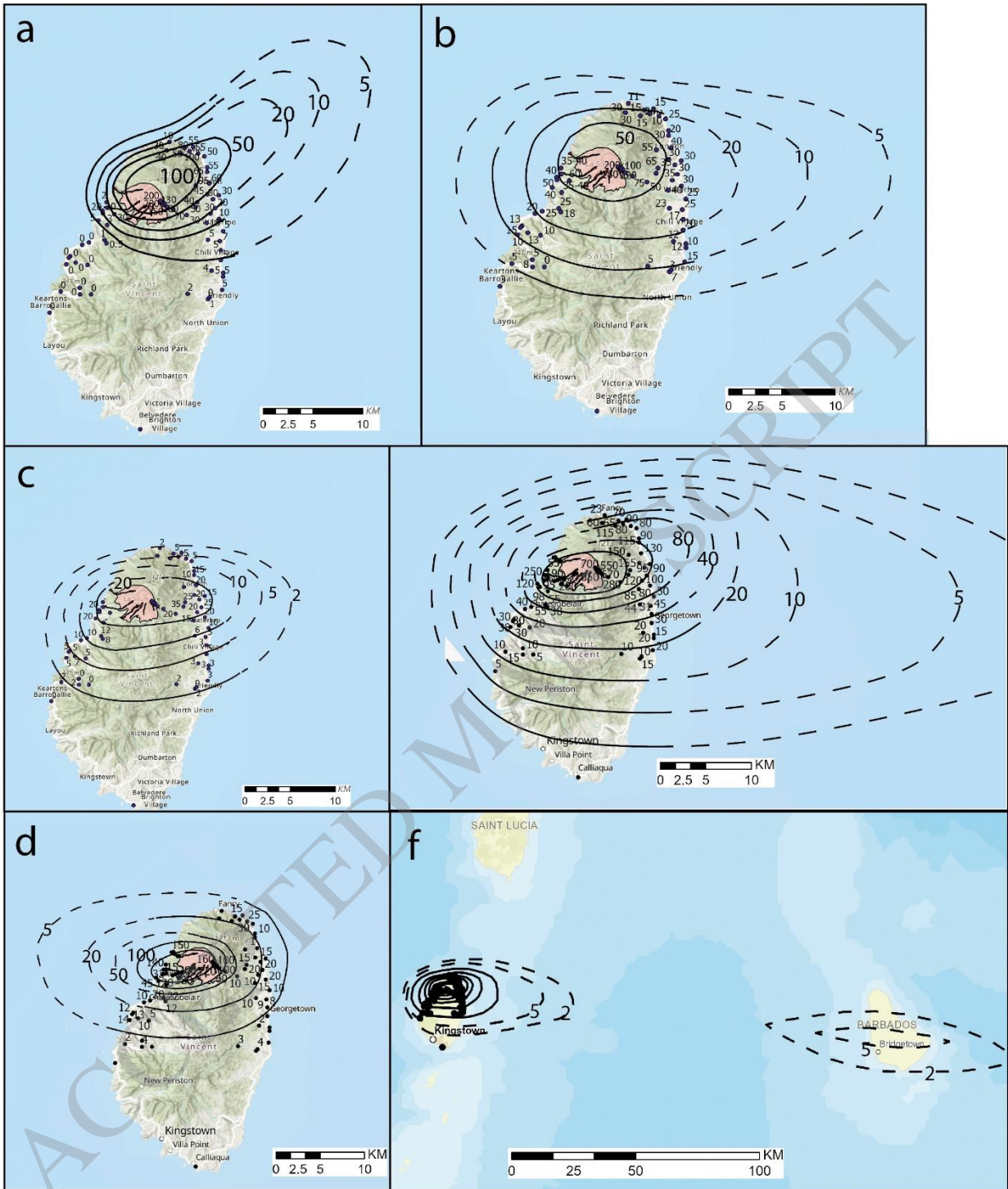


Figure 10

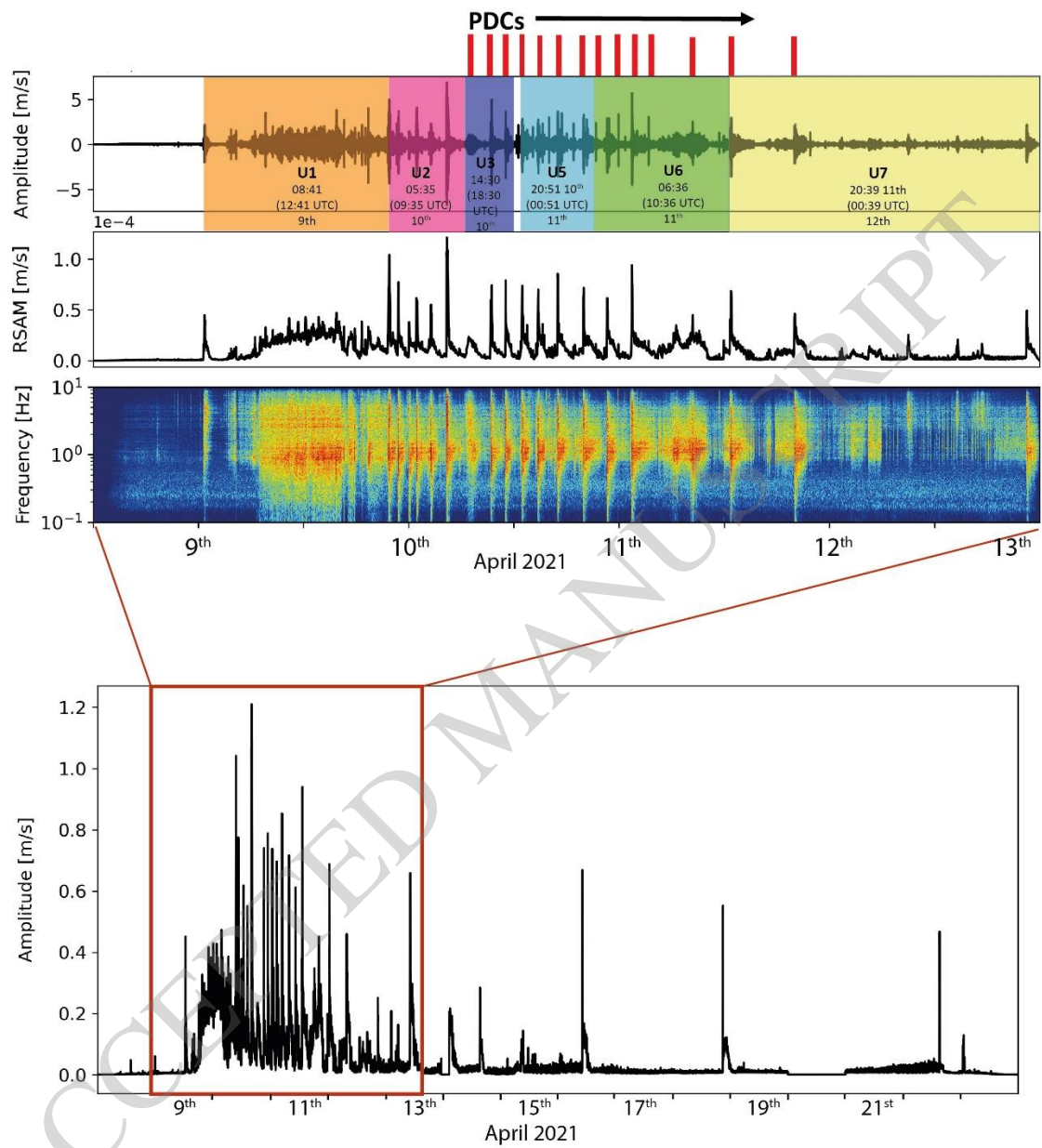


Figure 11

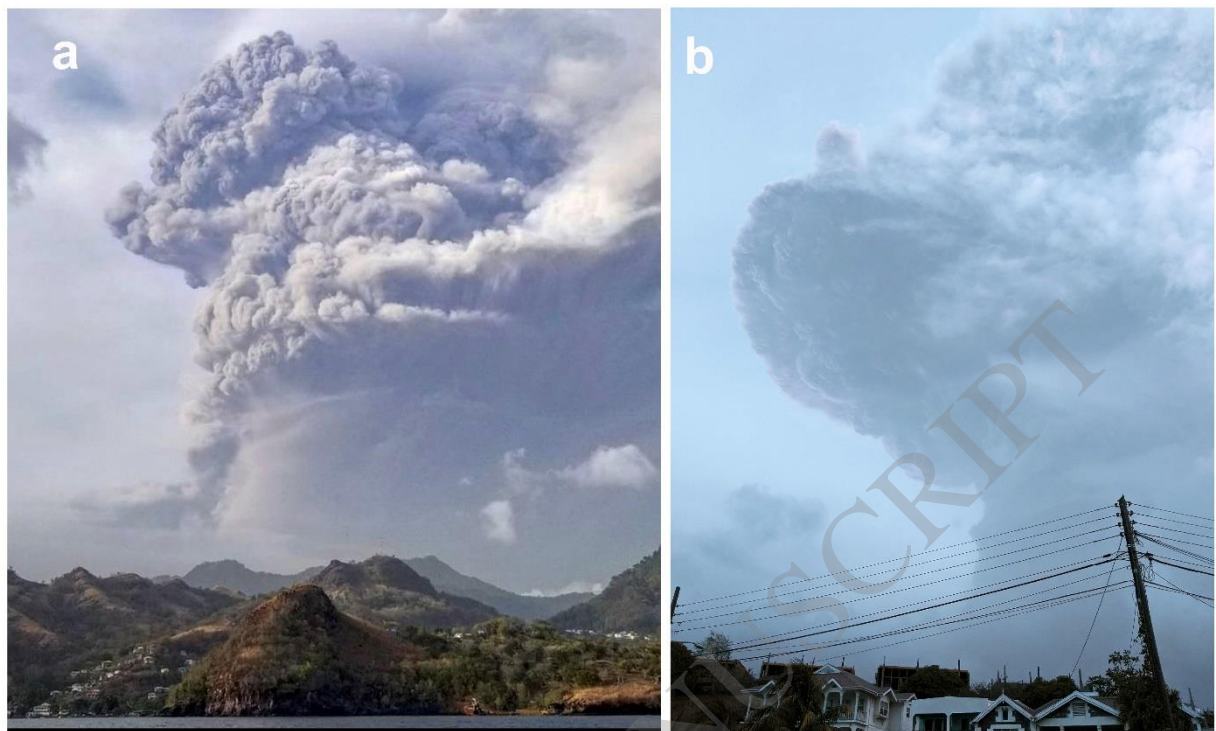


Figure 12